Functional and evolutionary perspectives on gill structures of an obligate air-breathing, aquatic snail

Cristian Rodriguez Equal first author, 1, 2, 3 , **Guido I Prieto** Equal first author, 3 , **Israel A Vega** Corresp., 1, 2, 3 , **Alfredo Castro-Vazquez** Corresp. 1, 2, 3

1 IHEM, CONICET, Universidad Nacional de Cuyo, Mendoza, Argentina

2 Instituto de Fisiología, Facultad de Ciencias Médicas, Universidad Nacional de Cuyo, Mendoza, Argentina

3 Departamento de Biología, Facultad de Ciencias Exactas y Naturales, Universidad Nacional de Cuyo, Mendoza, Argentina

Corresponding Authors: Israel A Vega, Alfredo Castro-Vazquez
Email address: israel.vega7@gmail.com, a.castrovazquez@gmail.com

Ampullariids are freshwater gastropods bearing a gill and a lung, thus showing different degrees of amphibiousness. In particular, *Pomacea canaliculata* (Caenogastropoda, Ampullariidae) is an obligate air-breather that relies mainly or solely on the lung for dwelling in poorly oxygenated waters, for avoiding predators, while burying in the mud during aestivation, and for oviposition above water level. In this paper, we studied the morphological peculiarities of the gill in this species. We found (1) the gill and lung vasculature and innervation are intimately related, allowing alternation between water and air respiration; (2) the gill epithelium has features typical of a transporting rather than a respiratory epithelium; and (3) the gill has resident granulocytes within intraepithelial spaces that may serve a role for immune defence. Thus, the role in oxygen uptake may be less significant than the roles in ionic/osmotic regulation and immunity. Also, our results provide a morphological background to understand the dependence on aerial respiration of *P. canaliculata*. Finally, we consider these findings from a functional perspective in the light of the evolution of the water-to-land transition in the Ampullariidae, and discuss that master regulators may explain the phenotypic convergence of gill structures amongst this molluscan species and those in other phyla.

Functional and evolutionary perspectives on gill structures of an obligate air-breathing, aquatic snail

Cristian Rodriguez[1,2,3†], Guido I Prieto[3†], Israel A Vega[1,2,3*], Alfredo Castro-Vazquez[1,2,3*]

[1] IHEM, CONICET, Universidad Nacional de Cuyo, Mendoza, Argentina.
[2] Universidad Nacional de Cuyo, Facultad de Ciencias Médicas, Instituto de Fisiología, Mendoza, Argentina.
[3] Universidad Nacional de Cuyo, Facultad de Ciencias Exactas y Naturales, Departamento de Biología, Mendoza, Argentina.

[†]These authors contributed equally to this work.

* Corresponding Authors
Alfredo Castro-Vazquez
Centro Universitario, Mendoza, Casilla de Correo 33, 5500, Argentina
Email address: a.castrovazquez@gmail.com
Israel A. Vega
Centro Universitario, Mendoza, Casilla de Correo 33, 5500, Argentina
Email address: iavega.conicet@gmail.com

Abstract

Ampullariids are freshwater gastropods bearing a gill and a lung, thus showing different degrees of amphibiousness. In particular, *Pomacea canaliculata* (Caenogastropoda, Ampullariidae) is an obligate air-breather that relies mainly or solely on the lung for dwelling in poorly oxygenated waters, for avoiding predators, while burying in the mud during aestivation, and for oviposition above water level. In this paper, we studied the morphological peculiarities of the gill in this species. We found (1) the gill and lung vasculature and innervation are intimately related, allowing alternation between water and air respiration; (2) the gill epithelium has features typical of a transporting rather than a respiratory epithelium; and (3) the gill has resident granulocytes within intraepithelial spaces that may serve a role for immune defence. Thus, the role in oxygen uptake may be less significant than the roles in ionic/osmotic regulation and immunity. Also, our results provide a morphological background to understand the dependence on aerial respiration of *P. canaliculata*. Finally, we consider these findings from a functional perspective in the light of the evolution of the water-to-land transition in the Ampullariidae, and discuss that master regulators may explain the phenotypic convergence of gill structures amongst this molluscan species and those in other phyla.

Introduction

Respiratory organs are identified as either gills or lungs, whether they are formed as protrusions or as invaginations of the respiratory mucosae. Gills are almost always used for aquatic respiration, while lungs are for aerial respiration, but in addition to their respiratory functions, these organs may also serve other functions (Maina 2000a; Maina 2002b).

In bimodal breathers (i.e. aquatic animals that have retained a gill while having a respiratory organ for breathing air), the gill may partially lose the respiratory role while acquiring other roles. In such cases, the respiratory function is supplied mainly by the air-breathing organ: in bimodal crustaceans and fishes, for example, the dependence on water comes in grades, the lesser water-dependent species having well-developed lungs that take up oxygen from the air and have reduced or modified gills for ionic/osmotic regulation and CO_2 excretion (Farrelly & Greenaway 1987; Graham et al. 2007; Hughes & Morgan 1973; Innes & Taylor 1986; Low et al. 1988).

Most gastropods are marine and bear ctenidial gills (Haszprunar 1988), but some have adapted to terrestrial and freshwater life by developing lungs, as different specialisations of the mantle cavity, which occur in the Panpulmonata (Heterobranchia) and the Ampullariidae (Caenogastropoda). The latter is a family of bimodal breathers that have retained a gill, but in which the lung allows them to breathe air, thus showing different degrees of amphibiousness (Hayes et al. 2015). As it occurs in bimodal crustaceans and fishes, ampullariids vary in their dependence on water, being the genera *Afropomus*, *Saulea*, *Lanistes*, *Asolene*, *Felipponea*, and *Marisa* more water-dependent than *Pila* and *Pomacea* (Hayes et al. 2009a; Robson 1922).

Pomacea canaliculata (Lamarck 1822) is an obligate air-breather that has a well-developed lung and a siphon, which uses as a snorkel to ventilate the lung while being submerged (Andrews 1965). Behavioural observations have shown that *P. canaliculata* relies mainly or solely on the lung for dwelling in poorly oxygenated waters, for avoiding predators (Ueshima & Yusa 2014), while burying in the mud during aestivation (d'Orbigny 1847; Giraud-Billoud et al. 2011; Giraud-Billoud et al. 2013b; Hayes et al. 2015), and for oviposition above water level (Hayes et al. 2009b).

These facts make *P. canaliculata* (and the Ampullariidae in general) interesting models to investigate the suitability of respiratory organs for the exchange of gases as well as the structural and functional integration of both respiratory organs. In a far-reaching perspective, such studies can help us understand the evolution of terrestriality.

In this paper, we present a thorough description of the gill of *P. canaliculata* at the anatomical (3D rendering of its circulation), histological and ultrastructural levels. This is the first transmission electron microscopy study of a gill in the Caenogastropoda. Also, we discuss the significance of our findings from a functional and evolutionary perspective, because we were stricken by the morphological parallelisms found between the gill of *P. canaliculata* and those of somewhat phylogenetically distant taxa.

Materials and methods

Animals and culturing conditions

Animals were obtained from the Rosedal strain of *P. canaliculata*, whose origin and culture conditions have been described several times elsewhere (e.g., Cueto et al. 2015; Rodriguez et al. 2018). Procedures for snail culture, sacrifice, and tissue sampling were approved by the Institutional Committee for the Care and Use of Laboratory Animals (Comité Institucional para el Cuidado y Uso de Animales de Laboratorio (CICUAL), Facultad de Ciencias Médicas, Universidad Nacional de Cuyo), Approval Protocol N° 55/2015.

Light microscopy

Adult animals were immersed in water at 4°C for 20–30 minutes both for relaxation and minimizing pain, before careful shell cracking. Then, pieces of the gill (N = 6) were dissected

out and fixed in diluted (1:2) Bouin's fluid. Afterwards, they were dehydrated in a graded ethanol series, cleared in xylene and embedded in a 1:1 paraffin–resin mixture (Histoplast®, Argentina). Sections (3–5 µm thick) were obtained, stained with Gill's haematoxylin and eosin. ~~Similarly~~ processed samples were used for 3D rendering of the branchial architecture (see next Section).

Also, small pieces of the gill (N = 6) were fixed in Karnovsky's fluid (4% paraformaldehyde, 2.5% glutaraldehyde, dissolved in 0.1 M phosphate buffer, pH 7.4). One day later, tissues were washed thrice in phosphate buffer and transferred to 1% osmium tetroxide overnight. Afterwards, they were gradually dehydrated in a graded acetone series and finally embedded in Spurr's resin. Ultramicrotome sections (~200 nm) were stained with toluidine blue and mounted with DPX medium (Sigma-Aldrich, Cat. #44581). The stained sections were examined and photographed under a Nikon Eclipse 80i microscope using Nikon DS-Fi1-U3 camera and Nikon NIS-ELEMENT Image Software for image acquisition. Also, Karnovsky-fixed samples were used for transmission electron microscopy, as described below.

Computerised 3D rendering of gill circulation and innervation

The gill, lung and pericardium were dissected as a single piece from two young adult males (20 mm shell length). This material was fixed and embedded as described above; the lung was collapsed before fixation to reduce the size of the piece. Serial sections (10 µm thick) were stained with Gill's haematoxylin and eosin and photographed with a Nikon Digital Sight DS-5M camera on a Nikon Alphaphot-2 YS2 microscope. Digital images from one every ~~five~~ sections were manually aligned and the 3D-rendering of structures was performed using Reconstruct, version 1.1.0.0 (Fiala 2005), downloaded from Synapse Web, Kristen M. Harris, PI (http://synapses.clm.utexas.edu). Preparation of the PDF-3D-model was accomplished following published procedures (Ruthensteiner 2008; Ruthensteiner & Hess 2008) using the 3D components of Adobe Acrobat 9 Pro Extended software.

Scanning electron microscopy

Samples of the gill (N = 6) were dissected out and fixed in diluted Bouin's fluid (1:2) and were serially dehydrated in ethanol, passed through acetone and then critical point dried, mounted on aluminium stubs, coated with gold, and examined with a Jeol/EO JSM-6490LV scanning electron microscope.

Transmission electron microscopy

Ultrathin sections of gill samples fixed in Karnovsky's fluid and embedded in Spurr's resin were mounted on copper grids and stained with uranyl acetate and lead citrate, and examined with a Zeiss EM 900 transmission electron microscope.

Results

~~T~~he gill and related pallial organs

The respiratory organs in the pallial complex are the gill and the lung. In addition, there are other organs that serve an accessory function, namely the siphon, the right nuchal lobe, and the 'mantle fold', which are depicted in Fig. 1A.

The gill extends from the left rear end of the mantle cavity (in the proximity of the pericardium and next to the ureter) to the right front side of the mantle cavity, close to the anus and the copulatory apparatus and limits on its left and anterior sides with the saccular lung (Fig.

1A). The gill is formed by a single row of rather parallel leaflets (i.e. a ctenidial monopectinate condition) that hang from their bases in the mantle cavity's roof, in which the main afferent and efferent vessels run (Fig. 1B).

The lung extends through most of the mantle cavity's roof and communicates with the mantle cavity through the pneumostome, close to the underlying air-breathing siphon, which is homologous to the left nuchal lobe –and not to the water-inhalant siphon– of other caenogastropods (Ponder & Lindberg 1997).

The 'pallial fold' (Andrews 1965) is a mucosal ridge that extends on the floor of the mantle cavity. It originates at the left posterior end of the mantle cavity, close to the pericardium, and runs to the right until it crosses the prostate (or the vagina in females) and then takes a diagonal anteroposterior direction towards the proximity of the right nuchal lobe. A functionally significant narrow groove is delimited between this fold, the gill, and the rear wall of the mantle cavity. An exhalant water stream flows through the course of the groove, thus expelling urine and faeces (Andrews 1965).

The right nuchal lobe appears in fixed specimens as a short mucosal triangular fold hanging from the right side of the neck (Fig. 1A). In living animals, however, it is a thin scoop-like structure, which may occlude partly or totally the excretory mantle opening.

Blood circulation in the gill

The 3D rendering showed the *afferent branchial vessel* collects blood from ureteral efferents, particularly the *efferent ureteral vessel*. Additionally, other gill afferents come from *rectal* and *right pallial vessels* and *sinuses* that drain blood from the visceral hump. These afferents join the *afferent branchial vessel*, which continues as the *afferent pulmonary vessel*. Blood from the *afferent branchial vessel* flows through the gill leaflets to the *efferent pulmobranchial vessel* and then to the heart auricle, or alternatively, to the *ventral afferent pulmonary vessel* that irrigates the right half of the lung floor (Figs. 2A–C and Supplemental Fig. S1), thus integrating branchial and pulmonary circulation.

The haemocoel within each leaflet extends as a perforated fluid lamina between both lateral surfaces of the leaflet, and is identified here as the *laminar leaflet sinus*. However, there are also two rather continuous haemocoelic sinuses in each leaflet: a *marginal leaflet sinus* runs along the free border of each leaflet, while the other, namely the *basal leaflet sinus*, extends at the base of the gill as a short cut between the *afferent branchial vessel* and the *efferent pulmobranchial vessel*. These sinuses communicate extensively with the *laminar leaflet sinus*, which also connects with the *ventral afferent pulmonary vessel* (Fig. 2D–F and Supplemental Fig. S1).

Branchial nerves and their origins

Innervation of the gill of *P. canaliculata* comes from the *supraintestinal ganglion* and an *accessory supraintestinal ganglion* (only mentioned by Ghosh, 1912 for *Pila globosa*) that is located in the course of the *viscero–supraintestinal connective*. These origins are diagrammatically shown in Fig. 3A.

Nerve branches of the *branchial nerve* arising from the *supraintestinal ganglion* go through the lung roof (perhaps giving off neurites that innervate the lung roof) and end at the base of the gill leaflets. Each leaflet, however, shows a nerve accompanying the skeletal rod (Fig. 3B). These *leaflet nerves* apparently originate from branches of the *branchial nerve*.

The *accessory supraintestinal ganglion* is a thickening of the *viscero–supraintestinal connective*, which lies close to the pericardium, and that gives off a nerve longitudinally traversing the ureter and running along the base of the gill, next to the *afferent branchial vessel*. The latter nerve has not been referred for *P. canaliculata* (or for any other ampullariid) and it is here referred to as the *branchial base nerve*, which accompanies the *afferent branchial vessel*, and is shown in Fig. 3C.

Also, neurite bundles arising from the *copulatory ganglion* are likely to join the *branchial base nerve* through its anterior end (Fig. 3C), at least in male animals. The *copulatory ganglion* lies close to the gill's anterior end, in the proximity of the anus and the copulatory apparatus (Giraud-Billoud et al. 2013a).

The gill leaflet and its regions

The shape of a leaflet reminds a shark's inverted dorsal fin (Fig. 4). Each leaflet is covered by a columnar epithelium and it is supported by a skeletal rod accompanied by a *leaflet nerve*, which is in contact with the *marginal leaflet sinus*.

Four regions may be distinguished in each leaflet that are characterised by different epithelia (Figs. 4 and 5). A summary of data is provided in Table 1.

Under scanning electron microscopy, region I appears covered by microvillar cells, with interspersed ciliary cells (Fig. 5A), whereas regions III and IV are respectively covered with cells bearing either long (Fig. 5B) or short cilia (Fig. 5C). Region II differs from region I in that it shows no ciliary cells.

The *laminar leaflet sinus* occupies the central space of each leaflet and is limited by a thin fibromuscular layer, which underlies the epithelium. The sinus is traversed by trabeculae (Fig. 5D), which are thinner in regions I and II than in region III.

Epithelial cell types

The epithelium varies widely in the different regions of each leaflet (data are summarized in Table 2). In region I, it is columnar or low columnar (20–40 μm), and it is mainly composed of either clear or dark microvillar, mitochondria-rich cells (here referred to as α-cells and β-cells, respectively; Fig. 6). Besides that, there are also interspersed ciliary cells, and a lesser number of secretory cells. These cells (identified as C1, S1 and S2 cells, respectively) will be described for region IV, where they are more abundant.

Alpha-cells are characterised by euchromatic nuclei and conspicuous nucleoli. The cytoplasm contains numerous long mitochondria with well-defined cristae and glycogen deposits (Fig. 7A–C). Apically, these cells show few and rather short microvilli, and underlying membrane-bound bundles of electron-dense filaments/tubules. There is also a well-developed endomembrane vesicular system, as well as multivesicular (Fig. 7B) and multilamellar bodies (Fig. 7C).

Contrasting with α-cells, β-cells bear heterochromatic nuclei and a cytoplasm with numerous and tightly packed mitochondria (Fig. 7D–F). The surface area of the apical domain is increased by numerous and ramified microvilli, which somehow remind cauliflowers under the scanning electron microscope (see Fig. 5A). An apical narrow band of homogeneous cytoplasm is seen below the microvilli, together with the apical ends of an extensive tubular system, which extends to the underlying mitochondrial conglomerate (Fig. 7E). Multivesicular bodies as well as presumptively degenerative bodies, such as myeloid and fibrogranular figures, are also abundant in the perinuclear region of these cells (Fig. 7F). Alpha-cells and β-cells alternate in

approximately equal numbers. Numerous granulocytes lay inside epithelial intercellular spaces all along the leaflet's region I (Fig. 8), though they may also occur in other regions (see next Section).

A single cell type constitutes the epithelium in region III, which rests on a well-defined and electron-dense basal lamina (Fig. 9). It consists of cells with slender nuclei, very long cilia and short microvilli (C2 cells), and whose basolateral plasma membranes often enclose extensive and apparently dynamic intercellular spaces. The cytoplasm contains abundant rough endoplasmic reticulum and glycogen deposits (Fig. 9A–B). Transverse sections of cilia (Fig. 9C) show the typical 9+2 microtubule arrangement as well as membrane blebs (Fig. 9C, arrows). As α-cells, these cells have membrane-bound bundles of electron-dense filaments/tubules in the subapical region (Fig. 9D). Structures similar to these found in α and β cells of *P. canaliculata* have been shown in the gills of crustaceans (Maina 1990b) and larval amphibia (Brunelli et al. 2004), but with contrasting interpretations.

The epithelium in region IV rests on a well-defined and electron-dense basal lamina and exhibits the same cell types as epithelium in the region I, except for β-cells (Fig. 10A). However, ciliary C1 cells are the most abundant cell type here. They are characterised by a heterochromatic nucleus and an electron-dense cytoplasm that contains large dense-cored granules and glycogen deposits. The subapical region is similar to those of α-cells, but apically there are finger-like microvilli and short cilia (Fig. 10B). Secretory S1 cells are mucous cells with merging granules containing an electron-dense mesh above the nucleus (Fig. 10C), and granules with a looser electron-dense mesh in the apical domain (Fig. 10D). These granules would correspond to the densely and loosely metachromatic accumulations seen in toluidine blue preparations (Fig. 4E). The other type of secretory cells (S2 cells) have their cytoplasm almost filled with granules with a low electron-dense core, which are orthochromatic in toluidine blue preparations (Fig. 10E).

Epithelium in region II exhibits α-cells, and abundant S1 and S2 cells. Regions III and IV are those directly exposed to the incoming water current that flows over the gill, and both the long and short cilia may contribute to the water movement.

Apical intercellular junctions and the basolateral domain of epithelial cells

All epithelia examined showed two types of cellular junctions in an orderly fashion. Apical adherent junctions (also called *zonula adhaerens* or 'desmosome belt'; Fig. 11A) are followed by septate junctions (Fig. 11B), which are often interrupted by intercellular canaliculi (Fig. 11A–B), as those found in transporting epithelia (Cioffi 1984). Rather frequently, the canaliculi contain a globular, unidentified material. Below the septate junctions, the adjacent plasma membranes are separated by larger spaces, which increase in size towards the basal domain (Fig. 11C).

The basolateral domain of epithelial cells in all regions of a leaflet is a labyrinth of intermingled thin extensions that project towards the underlying connective tissue. There are conspicuous spaces between epithelial cells, which are frequently occupied by granulocytes (Fig. 8). Small neurite bundles, with or without accompanying glial cells, are also found into the intercellular spaces, thus providing direct intraepithelial innervation. A collagen matrix and sparse muscle fibres form the underlying connective tissue, which delimits the leaflet haemocoel. Neurite bundles accompanied by glial cells are frequently found in this tissue (see Fig. 8A), and these will be further described in next Section.

A notable feature of this epithelium is the occurrence of granulocytes, with eccentric nuclei and conspicuous nucleoli, the characteristic R granules (Cueto et al. 2015), and areas of glycogen deposits. Granulocytes are often fully enclosed into expanded intercellular spaces (Fig. 8A–B),

but sometimes, discontinuities in the mesh of basal projections of epithelial cells are found. These discontinuities communicate the intercellular spaces directly with the basal lamina, which is evident by means of its well-delimited *lamina densa* with interspersed electron-dense thickenings (Fig. 8C).

Fibromuscular tissue, skeletal rod and fine innervation

Underlying the basal lamina there are muscle cells embedded in a collagen matrix. These muscle cells show myofibrils and scarce mitochondria. The cell surface shows numerous electron-dense anchoring junctions composed of an external brush-like plaque and an internal amorphous but electron-dense layer. The fibrils of the brush-like plaques are often continuous with those of other cells' plaques or with thickenings of the *lamina densa* (Fig. 12A–B). These peculiar structures lie over clear cytoplasmic areas, which are traversed by thin cytoskeletal fibres. Similar structures have been described by Nakao (1975) in the trabecular cells of a bivalve. In *P. canaliculata*, these cells may correspond to the anchoring part of the trabeculae shown in Fig. 4.

Numerous neurite bundles that traverse the connective tissue and sometimes go into the epithelial intercellular spaces provide leaflet innervation. Neurites form bundles that are flanked by glial cell processes (Fig. 12C). Glial cells, or less frequently, uncovered neurites are in contact with muscle cells. Glial cells have rounded electron-dense, membrane-bound, granules of two different sizes (either ~400 nm or ~100 nm wide). Neurites have an electron-lucent axoplasm with neurofilaments. Fibre enlargements (presumptive nerve endings) contain ~80 nm wide granules of variable electron density and ~50 nm wide clear vesicles (Fig. 12C), which would indicate the existence of more than one neurotransmitter.

The *leaflet nerve* (Fig. 13A) runs along the free margin of each leaflet. In the efferent part, beneath epithelial region IV, it is accompanied by a sheath of muscle fibres. This sheath, that has some rigidity and constitutes a well-defined unit (Fig. 13B), seems homologous to the skeletal rod found in some other gastropods (Haszprunar 1988). At closer examination, the *leaflet nerve* is formed by tightly packed neurites and some glial processes (Fig. 13C–D), whereas the skeletal rod is formed by large muscle fibres immersed in a dense collagen matrix (Fig. 13E).

Discussion

The gill as a respiratory organ

An efficient respiratory organ requires a both large and thin surface area. This respiratory surface should be fully exposed to the external medium to allow gas exchange (Maina & West 2005). Indeed, in the extreme case of an aquatic animal being brought to air, the gill leaflets tend to stick together thus decreasing the surface area for the gas exchange, and hence, leading the animal to asphyxia (Maina 2002b). Therefore, to permit an adequate gas exchange, some mechanical rigidity to support a deployed gill is indispensable. Different structures have evolved to support the weight of gills, such as the cartilaginous or bony supporting rods (gill rays) and the interbranchial septa in fishes (Evans et al. 2005), the cuticle and the intralamellar septa in crustaceans (e.g., Farrelly & Greenaway 1987; Farrelly & Greenaway 1992), and the skeletal rods in some molluscs (Haszprunar 1988).

According to the latter author, skeletal rods have arisen several times in the evolution of molluscs in general, and twice amongst gastropods, namely in the Vetigastropoda and in the Ampullariidae (Caenogastropoda). These rods are supporting structures along the efferent border of gill leaflets, that Hyman (1967) had already referred for the vetigastropods' families Haliotidae, Trochidae, and Fissurellidae. Furthermore, Wanichanon et al. (2004) have reported

the rod of *Haliotis asinina* (Haliotidae) as a 'chitinous' structure which was accompanied by a muscle bundle, and also Eertman (1996) mentioned the existence of a rod in the gill leaflets of *Austrocochlea constricta* (Trochidae), but he did not study its ultrastructure.

Though the leaflet's skeletal rod of the Ampullariidae has been mentioned several times (Berthold 1991; Haszprunar 1988; Ponder & Lindberg 1997; Salvini-Plawen & Haszprunar 1987), no information on its microstructure was given in those papers. Furthermore, we are not aware of reports of a rod in the related caenogastropod families Cyclophoridae and Viviparidae, which together with the Ampullariidae, conform the 'informal group' Architaenioglossa (Caenogastropoda) (sensu Bouchet et al. 2005). In *P. canaliculata*, we here show that a skeletal rod occurs in the efferent margin of each gill leaflet. It is U-shaped in sections and is made of large muscle fibres, embedded in a collagen matrix (see Fig. 13), i.e. it is a contractile structure, and not merely 'chitin' (Wanichanon et al. 2004) or collagen (Hyman 1967). It accompanies the *leaflet nerve* and the *marginal leaflet sinus*.

The muscular skeletal rod would keep the leaflet deployed to expose its efferent margin to the water current passing from left to right through the mantle cavity. Besides that, ciliary beating should conduct water between the leaflets towards the mantle groove, according to Andrews' (1965) observations on fresh material. In this way, a countercurrent mechanism would occur between blood flowing through the leaflets and water flowing between them, facilitating the O_2 extraction from water (see Fig. 2F). Gill leaflets have a single laminar sinus pierced by trabeculae and bounded by continuous sinuses at the leaflet borders and base, but with no transverse sinuses as interpreted by Andrews (1965). This laminar arrangement implies a slow sheet-flow of blood, which likely facilitates the exchange of respiratory gases (Maina 2000b; Maina 2002a) and, perhaps more importantly, of ions. Moreover, this 'sheet-flow design' is in agreement with that found in other molluscan, crustacean, and fish gills (e.g., Booth 1978; Knight & Knight 1986; Maina 1990a).

However, in spite of having a countercurrent mechanism for O_2 extraction, the gas exchange should be hindered by the thickness of the gill epithelium (>20 μm), according to Fick's first law of diffusion (Maina & West 2005). Also the large number of mitochondria found in epithelial cells (see Figs. 6 and 7) indicates a high oxygen consumption, but this finding contradicts the idea that a respiratory tissue barrier must consume a minimal amount of the oxygen it extracts from the external medium (Maina 2000b). Indeed, a high oxygen consumption rate would be required for ion pumping against concentration gradients, which likely occurs in the gill epithelium, as discussed above.

It should be considered, however, that a decrease in septate junctions' length –as occurs in leaflet region III– may shorten the distance between the external and internal media for the passage of molecules via the paracellular pathway (Yu 2017). It is therefore expected that some downhill diffusion of gases followed this route, which requires no energy expenditure. However, the gill CO_2 excretion would be higher than the O_2 uptake, because of the higher solubility of CO_2 in water. This occurs, indeed, in many freshwater bimodal-breathing fishes (e.g., Evans et al. 2005) and crustaceans (e.g., Innes & Taylor 1986), in which CO_2 excretion occurs mainly through their gills.

Thus, in gill leaflets, deoxygenated blood coming from the *afferent branchial vessel* would reach the *basal and marginal leaflet sinuses* and would distribute through the *laminar leaflet sinus*, where incomplete oxygenation should happen (Fig. 2F). In this way, partially oxygenated blood would converge either to the *efferent pulmobranchial vessel* or the *ventral afferent pulmonary vessel*, as shown in Fig. 2F. The fact that partially oxygenated blood went directly to

the lung floor would prove to be useful to complete the O_2 uptake when the animal is submerged, because the gill might be insufficient to do that. Moreover, when on land, the collapse of leaflets and their laminar sinuses would force blood to follow the *basal* or *marginal sinuses* converging in the *ventral afferent pulmonary vessel* (Fig. 2F). In this way, there would be a shunt to the lung circulation, where oxygenation should reach its maximum (Maina 1990a).

Altogether, these features may determine *P. canaliculata* to be an obligate air-breathing species, whose gill structures seem better suited for ionic/osmotic regulation than for O_2 uptake. In fact, Seuffert & Martín (2010) showed that *P. canaliculata*'s micro distribution in the field is mostly restricted to 2–4 m from the nearest emergent substratum, and that impeding aerial respiration negatively affected its survivorship in aquaria.

The gill as an ionic/osmotic regulator

P. canaliculata is a hyperosmotic and hyperionic regulator (Cueto et al. 2011) and, like in many other freshwater animals, its gill may be involved in this regulation. Indeed, the gill has a high ion-ATPase activity (Taylor & Andrews 1987), which suggests it is a site of ion uptake from the surrounding water, while the ureter would be a site of ion reabsorption from the primary urine (Taylor & Andrews 1987).

As discussed above, the gill epithelium of *P. canaliculata* (Fig. 4) is characterised by tall columnar cells with apical specialisations, numerous mitochondria, and basolateral infoldings of the plasma membrane that enclose broad and presumably dynamic intercellular spaces. Additionally, these highly polarised cells have well-developed endomembrane systems and glycogen deposits (see Figs. 6 and 7). It is worth mentioning that there is not a zone covered by pavement cells as it may be found in fishes (Evans et al. 2005). Taken together, these features contrast with the gill respiratory epithelia found in some other molluscan (e.g., Fischer et al. 1990; Le Pennec et al. 1988; Manganaro et al. 2012; Nuwayhid et al. 1978) and non-molluscan taxa (e.g., Evans et al. 2005; Luquet et al. 2002) that are more dependent on water breathing, and which show cubic or squamous cells, with low nuclear/cytoplasmic ratios and a low content of mitochondria and other organelles. In turn, the gill structures found in *P. canaliculata* are more similar to those of transporting epithelia (Berridge & Oschman 2012), such as those of the vertebrate small intestine (e.g., Flik & Verbost 1993), gallbladder (e.g., Housset et al. 2016), and renal tubules (e.g., Yu 2017), and of the ionic/osmotic regulatory epithelia in the gills of crustaceans (e.g., Luquet et al. 2002; McNamara & Faria 2012) and fishes (e.g., McDonald et al. 1991).

There are two main morphological types of presumptive ion-transporting cells in *P. canaliculata*, which may be equivalent to the α and β mitochondria-rich cells found in freshwater teleost fishes (for a review, see Evans et al. 2005; Wilson & Laurent 2002) and to the 'fibrillar' and 'tubulovesicular' types found in amphibians (Lewinson et al. 1987). Both α- and β-cells of *P. canaliculata* are indeed mitochondria-rich cells. Like those of fishes, α-cells have an electron-lucent cytoplasm, an apical membrane slightly concave with few and short apical specialisations, and a well-developed subapical vesicular system (Figs. 6 and 7A). This cell type also resembles the amphibian 'fibrillar cells' because of its membrane-bound bundles of electron-dense filaments/tubules (Fig. 7B). On the other hand, β-cells have an electron-dense cytoplasm and complex apical specialisations of the plasma membrane (Figs. 6 and 7D), as fish β-cells do. They also have a well-developed tubulovesicular system that almost fills the cytoplasm between mitochondria (Fig. 7E), in close resemblance to the 'tubulovesicular' cell type of amphibians (Lewinson et al. 1987). It should be noted that the highlighted similarities between fish,

amphibian and *P. canaliculata*'s mitochondria-rich cell types suggest some similar regulatory mechanisms.

The gill as an immune barrier

In general, integumentary structures are the first barrier to microbial intruders, and as such, the gill is one of these structures preventing their access from the mantle cavity. In fact, *P. canaliculata* must also cope with the diverse symbiotic organisms that naturally dwell into the mantle cavity (Vega et al. 2006). Moreover, abundant mucus is found covering the gill epithelium, which is likely secreted by leaflets regions II and IV, where a large number of mucous cells occur (Figs. 4 and 10). Mucus secretion and water currents may be unfavourable for the settling of many organisms (Vega et al. 2006).

However, the gill is also a potential barrier because of its position in the circulation, as are the kidney and lung in *P. canaliculata* (Rodriguez et al. 2018). Indeed, most blood coming from the cephalopodal mass and the visceral hump has to pass through the gill before reaching the heart to re-enter the general circulation. Thus, the gill itself, beyond its role as part of the integumentary barrier, may also function as a filter for blood-borne microorganisms.

The conspicuous occurrence of granulocytes amongst epithelial intercellular spaces (Figs. 4 and 8) suggests these cells would serve in immune surveillance in this organ. The occurrence of immunocompetent cells within epithelial intercellular spaces is a widespread feature amongst the gills of bivalves (e.g., de Oliveira David et al. 2008; Gregory et al. 1996) and fishes (e.g., Hughes & Morgan 1973). The granulocytes found in the gill were larger than those found in the general circulation of *P. canaliculata* and, in spite of being the less frequent cell type in the circulation (see Cueto et al. 2015), the intercellular spaces had only granulocytes within them.

There is evidence of a kind of 'compound exocytosis' (Pickett & Edwardson 2006) leading to granulocyte degranulation in *P. canaliculata* (Cueto et al. 2015). Granulocyte degranulation in bivalves (e.g., Ciacci et al. 2009; Cheng et al. 1975; Foley & Cheng 1977; Mohandas et al. 1985; Rebelo et al. 2013) has been related to the release of lysozyme and other hydrolytic enzymes that may kill bacteria and fungi, and Ottaviani (1991) has reported lysozyme from haemocytes of a gastropod. Therefore, it is likely that granulocytes occurring into the intercellular spaces of the gill epithelium are there serving a defensive role against intruders in *P. canaliculata*.

Nervous control

The gill is mainly innervated from the *supraintestinal ganglion* (and the *accessory supraintestinal ganglion* found in *P. canaliculata*; see Fig. 3A), which are part of the ganglionar 'visceral loop' (Chase 2002) that also includes the subintestinal and the visceral ganglia (Berthold 1991; Hylton Scott 1957). The *branchial nerve* also innervates the osphradium and the muscular region of the lung that surrounds the pneumostome (C. Rodriguez, G.I. Prieto, I.A. Vega & A. Castro-Vazquez, unpubl. data). The osphradium has been shown to sense ionic or O_2/CO_2 levels in water, amongst other chemosensory functions in several gastropods (Lindberg & Sigwart 2015), and may be involved in the switching between the behavioural modes of branchial and lung respiration (C. Rodriguez, G.I. Prieto, I.A. Vega & A. Castro-Vazquez, unpubl. data), and in regulating the gill ionic/osmotic functions in *P. canaliculata*.

We have not found any neuroepithelial cells similar to those found in fish gills (Bailly et al. 1992; Dunel-Erb et al. 1982; Jonz & Nurse 2003). However, the neurite supply to the gill leaflets, which includes glial cell processes (Fig. 12C) similar to those referred by Nicaise (1973) in heterobranchs, is rich and spread in the connective tissue, the laminar sinus cells, and also in

the epithelial basolateral domain (see Fig. 3), as has been described in the gill leaflets of many fishes (e.g., Jonz & Zaccone 2009).

The sensory information coming from the osphradium and/or the gill epithelium may be integrated in the visceral loop and may trigger different responses through efferent pathways. For example, controlling the state of the intercellular spaces could either increase or decrease the epithelium permeability, thus regulating respiratory or ionic/osmotic functions, as there has been described in fish gills (e.g., Jonz & Nurse 2006). Efferent pathways may also be involved in the regulation of vascular resistance through the gill leaflets by altering the stretching of trabecular cells, as it occurs in pillar cells of fish gills (Jonz & Zaccone 2009). Indeed, numerous neurites were often found in close contact with these modified muscle cells (see Fig. 12). Finally, other motor innervation would involve that associated with the skeletal rod (see Fig. 13).

The bases of terrestriality: the family Ampullariidae as a case study

The family Ampullariidae has been proposed as a model for evolutionary biology because of its long evolutionary history that traces back to the Jurassic (~160 million years ago), wide geographic distribution (through Africa, Asia, and the Americas), and high diversity (~120 currently valid species) (Hayes et al. 2009a). These characteristics, along with the different degrees of amphibiousness ampullariids show, make this family an interesting model to study the evolution of terrestriality (Hayes et al., 2015). Important advances have been made in elucidating the evolution of traits related to terrestriality in Ampullariidae. In particular, the evolution of aerial oviposition (e.g., Hayes et al. 2009a; Ip et al. 2018; Mu et al. 2017) has received a considerable attention. However, a comparative study on the morphology, function, and development of the respiratory organs amongst the Ampullariidae is still lacking.

As mentioned above, the development of a lung has allowed a shift in the biological role of the gill to the detriment of its capacity for oxygen uptake in bimodal-breathing crustaceans and fishes. Our results suggest this may also be the case amongst the Ampullariidae and encourage the search for similar patterns through the comparison of the respiratory organs, and their relative functions, between ampullariid species with different degrees of terrestriality.

Finally, it is worth emphasising the convergence of gill structures of *P. canaliculata* with those in phylogenetically distant taxa, such as arthropods (e.g., Farrelly & Greenaway 1987; Luquet et al. 2002; Maina 1990a) and fishes (e.g., Evans et al. 2005; Laurent & Dunel 1980; Low et al. 1988; McDonald et al. 1991). Indeed, these may be cases of phenotypic convergence in which similar genetic mechanisms, such as the existence of conserved master regulators, can lead to convergence in form and function in independent and often distant lineages (Stern 2013). The existence of master regulators, such as the Hox and ParaHox genes, has been shown in representatives of seven classes of molluscs (De Oliveira et al. 2016). Future studies may be aimed at elucidating whether conserved master regulators are involved in the development of similar structures in the gill of *P. canaliculata*.

Upshot

Summarising:

1. We have confirmed interpretations of preceding authors regarding the vasculature and innervation of the gill of *P. canaliculata* and their implications. Namely, (a) that the gill vasculature is connected in series with that of the lung, in such a way that blood may complete oxygenation in the latter organ, and (b) that the origin of the gill innervation in the main and accessory supraintestinal ganglia supports the view of the adult's gill as the

post-torsional left gill, but which has been displaced to the right by the development of the lung.

2. When the animal is under water, the gill surface potentially available for gas exchange is large, but is covered by a rather thick epithelium (>20 μm), with no cubic or squamous cells as in the gills of crustaceans and fishes. Ultrastructural evidence suggests that the only structures that perhaps facilitate oxygen uptake would be those involved in the paracellular pathway.
3. Also, in case the branchial leaflets collapse when the animal is out of water, blood may bypass the leaflets and go directly to the lung through a shunt formed between the *basal branchial sinuses* and the *ventral afferent pulmonary vessel*.
4. The leaflet architecture is uniform throughout the whole gill, i.e. there is not a respiratory and ionic regionalisation of the gill as there occurs in other taxa (e.g., crustaceans).
5. Our findings indeed showed that the gill epithelium has features of a transporting epithelium rather than a respiratory one. Specifically, the branchial epithelium has (1) developed apical specialisations and basolateral infoldings, (2) occluding junctions, (3) extensive, and likely dynamic, intercellular spaces, (4) a high density of mitochondria, and (5) an underlying rich nerve supply. Altogether, these features suggest the gill in *P. canaliculata* would be more suitable for ionic/osmotic regulation than for oxygen uptake.
6. The gill may also function as an immune barrier by secreting mucus to prevent the access of intruders from the mantle cavity, but also to prevent the spread of blood-borne microorganisms, in which granulocytes may participate.

Acknowledgements

The authors appreciate the generous help of Elisa Bocanegra, Sergio A. Carminati, Norberto F. Domizio, Mabel Fóscolo, María Silvina Lassa, and María Paula López.

References

Andrews EB. 1965. The functional anatomy of the mantle cavity, kidney and blood system of some pilid gastropods (Prosobranchia). *Journal of Zoology* 146:70-94.

Bailly Y, Dunel-Erb S, and Laurent P. 1992. The neuroepithelial cells of the fish gill filament: Indolamine-immunocytochemistry and innervation. *The Anatomical Record* 233:143-161.

Berridge MJ, and Oschman JL. 2012. *Transporting epithelia*: Elsevier.

Berthold T. 1991. Vergleichende Anatomie, Phylogenie und historische Biogeographie der Ampullariidae (Mollusca, Gastropoda). *Abhandlungen des naturwissenschaftlichen Vereins in Hamburg* 29:1-257.

Booth JH. 1978. The distribution of blood flow in the gills of fish: application of a new technique to rainbow trout (*Salmo gairdneri*). *Journal of Experimental Biology* 73:119-129.

Bouchet P, Rocroi J-P, Frýda J, Hausdorf B, Ponder W, Valdés Á, and Warén A. 2005. Classification and nomenclator of gastropod families. *Malacologia* 47:1-397.

Brunelli E, Perrotta E, and Tripepi S. 2004. Ultrastructure and development of the gills in *Rana dalmatina* (Amphibia, Anura). *Zoomorphology* 123:203-211.

Ciacci C, Citterio B, Betti M, Canonico B, Roch P, and Canesi L. 2009. Functional differential immune responses of *Mytilus galloprovincialis* to bacterial challenge. *Comparative Biochemistry and Physiology Part B: Biochemistry and Molecular Biology* 153:365-371.

549 Cioffi M. 1984. Comparative ultrastructure of arthropod transporting epithelia. *American*
550 *Zoologist* 24:139-156.
551 Cueto JA, Giraud-Billoud M, Vega IA, and Castro-Vazquez A. 2011. Haemolymph plasma
552 constituents of the invasive snail *Pomacea canaliculata* (Caenogastropoda,
553 Architaenioglossa, Ampullariidae). *Molluscan Research* 31:57-60.
554 Cueto JA, Rodriguez C, Vega IA, and Castro-Vazquez A. 2015. Immune defenses of the
555 invasive apple snail *Pomacea canaliculata* (Caenogastropoda, Ampullariidae):
556 Phagocytic hemocytes in the circulation and the kidney. *PLoS ONE* 10:e0123964.
557 10.1371/journal.pone.0123964
558 Chase R. 2002. *Behavior and its neural control in gastropod molluscs.* Oxford: Oxford
559 University Press.
560 Cheng TC, Rodrick GE, Foley DA, and Koehler SA. 1975. Release of lysozyme from
561 hemolymph cells of *Mercenaria mercenaria* during phagocytosis. *Journal of Invertebrate*
562 *Pathology* 25:261-265.
563 d'Orbigny A. 1847. Voyage dans l'Amérique Méridionale. Paris: C.P. Bertrand. p 711.
564 De Oliveira AL, Wollesen T, Kristof A, Scherholz M, Redl E, Todt C, Bleidorn C, and
565 Wanninger A. 2016. Comparative transcriptomics enlarges the toolkit of known
566 developmental genes in mollusks. *BMC Genomics* 17:905.
567 de Oliveira David JA, Salaroli RB, and Fontanetti CS. 2008. Fine structure of *Mytella falcata*
568 (Bivalvia) gill filaments. *Micron* 39:329-336.
569 Dunel-Erb S, Bailly Y, and Laurent P. 1982. Neuroepithelial cells in fish gill primary lamellae.
570 *Journal of Applied Physiology* 53:1342-1353.
571 Eertman RHM. 1996. Comparative study on gill morphology of gastropods from Moreton Bay,
572 Queensland. *Molluscan Research* 17:3-20.
573 Evans DH, Piermarini PM, and Choe KP. 2005. The multifunctional fish gill: dominant site of
574 gas exchange, osmoregulation, acid-base regulation, and excretion of nitrogenous waste.
575 *Physiological Reviews* 85:97-177.
576 Farrelly C, and Greenaway P. 1987. The morphology and vasculature of the lungs and gills of
577 the soldier crab, *Mictyris longicarpus*. *Journal of Morphology* 193:285-304.
578 Farrelly CA, and Greenaway P. 1992. Morphology and ultrastructure of the gills of terrestrial
579 crabs (Crustacea, Gecarcinidae and Grapsidae): Adaptations for air-breathing.
580 *Zoomorphology* 112:39-49.
581 Fiala JC. 2005. Reconstruct: a free editor for serial section microscopy. *Journal of Microscopy*
582 218:52-61.
583 Fischer FP, Alger M, Cieslar D, and Krafczyk HU. 1990. The chiton gill: Ultrastructure in
584 *Chiton olivaceus* (Mollusca, Polyplacophora). *Journal of Morphology* 204:75-87.
585 Flik G, and Verbost P. 1993. Calcium transport in fish gills and intestine. *Journal of*
586 *Experimental Biology* 184:17-29.
587 Foley DA, and Cheng TC. 1977. Degranulation and other changes of molluscan granulocytes
588 associated with phagocytosis. *Journal of Invertebrate Pathology* 29:321-325.
589 Ghosh E. 1912. On the nervous system of *Ampullaria globosa*. *Records of the Indian Museum*
590 7:77-82.
591 Giraud-Billoud M, Abud M, Cueto J, Vega I, and Castro-Vazquez A. 2011. Uric acid deposits
592 and estivation in the invasive apple-snail, *Pomacea canaliculata*. *Comparative &*
593 *Biochemical Physiology Part A* 158:506-512.

Giraud-Billoud M, Gamarra-Luques C, and Castro-Vazquez A. 2013a. Functional anatomy of male copulatory organs of *Pomacea canaliculata* (Caenogastropoda, Ampullariidae). *Zoomorphology* 132:129-143.

Giraud-Billoud M, Vega IA, Rinaldi Tosi ME, Abud MA, Calderón ML, and Castro-Vazquez A. 2013b. Antioxidant and molecular chaperone defenses during estivation and arousal in the South American apple-snail *Pomacea canaliculata*. *Journal of Experimental Biology* 216:614-622.

Graham J, Lee H, and Wegner N. 2007. Transition from water to land in an extant group of fishes: Air breathing and the acquisition sequence of adaptations for amphibious life in Oxudercine gobies. In: Fernandes MN, Rantin FT, Mogens LG, and Kapoor B, eds. *Fish Respiration and Environment*: Science Publishers, 255-288.

Gregory M, George R, and McClurg T. 1996. The architecture and fine structure of gill filaments in the brown mussel, *Perna perna*. *African Zoology* 31:193-207.

Haszprunar G. 1988. On the origin and evolution of major gastropod groups, with special reference to the Streptoneura. *Journal of Molluscan Studies* 54:367-441.

Hayes KA, Burks R, Castro-Vazquez A, Darby PC, Heras H, Martín PR, Qiu J-W, Thiengo SC, Vega IA, Yusa Y, Wada T, Burela S, Cadierno MP, Cueto JA, Dellagnola FA, Dreon MS, Frassa VM, Giraud-Billoud M, Godoy MS, Ituarte S, Koch E, Matsukura K, Pasquevich Y, Rodriguez C, Saveanu L, Seuffert ME, Strong EE, Sun J, Tamburi NE, Tiecher MJ, Turner RL, Valentine-Darby P, and Cowie RH. 2015. Insights from an integrated view of the biology of apple snails (Caenogastropoda: Ampullariidae). *Malacologia* 58:245-302.

Hayes KA, Cowie RH, Jørgensen A, Schultheiß R, Albrecht C, and Thiengo SC. 2009a. Molluscan models in evolutionary biology: Apple snails (Gastropoda: Ampullariidae) as a system for addressing fundamental questions. *American Malacological Bulletin* 27:47-58.

Hayes KA, Cowie RH, and Thiengo SC. 2009b. A global phylogeny of apple snails: Gondwanan origin, generic relationships, and the influence of outgroup choice (Caenogastropoda: Ampullariidae). *Biological Journal of the Linnean Society* 98:61-76.

Housset C, Chrétien Y, Debray D, and Chignard N. 2016. Functions of the gallbladder. *Comprehensive Physiology* 6:1549-1577.

Hughes G, and Morgan M. 1973. The structure of fish gills in relation to their respiratory function. *Biological Reviews* 48:419-475.

Hylton Scott MI. 1957. Estudio morfológico y taxonómico de los ampulláridos de la República Argentina. *Revista del Museo Argentino de Ciencias Naturales "Bernardino Rivadavia"* 3:233-333.

Hyman LH. 1967. *The Invertebrates*. New York: McGraw-Hill.

Innes A, and Taylor E. 1986. The evolution of air-breathing in crustaceans: A functional analysis of branchial, cutaneous and pulmonary gas exchange. *Comparative Biochemistry and Physiology Part A: Physiology* 85:621-637.

Ip JC, Mu H, Zhang Y, Sun J, Heras H, Chu KH, and Qiu J-W. 2018. Understanding the transition from water to land: Insights from multi-omic analyses of the perivitelline fluid of apple snail eggs. *Journal of Proteomics*.

Jonz MG, and Nurse CA. 2003. Neuroepithelial cells and associated innervation of the zebrafish gill: a confocal immunofluorescence study. *Journal of Comparative Neurology* 461:1-17.

Jonz MG, and Nurse CA. 2006. Epithelial mitochondria-rich cells and associated innervation in adult and developing zebrafish. *Journal of Comparative Neurology* 497:817-832.
Jonz MG, and Zaccone G. 2009. Nervous control of the gills. *Acta Histochemica* 111:207-216.
Knight J, and Knight R. 1986. The blood vascular system of the gills of *Pholas dactylus* L.(Mollusca, Bivalvia, Eulamellibranchia). *Philosophical Transactions of the Royal Society of London B* 313:509-523.
Laurent P, and Dunel S. 1980. Morphology of gill epithelia in fish. *American Journal of Physiology-Regulatory, Integrative and Comparative Physiology* 238:R147-R159.
Le Pennec M, Beninger P, and Herry A. 1988. New observations of the gills of *Placopecten magellanicus* (Mollusca: Bivalvia), and implications for nutrition. *Marine Biology* 98:229-237.
Lewinson D, Rosenberg M, and Warburg M. 1987. Ultrastructural and ultracytochemical studies of the gill epithelium in the larvae of *Salamandra salamandra* (Amphibia, Urodela). *Zoomorphology* 107:17-25.
Lindberg DR, and Sigwart JD. 2015. What is the molluscan osphradium? A reconsideration of homology. *Zoologischer Anzeiger-A Journal of Comparative Zoology* 256:14-21.
Low W, Lane D, and Ip Y. 1988. A comparative study of terrestrial adaptations of the gills in three mudskippers: *Periophthalmus chrysospilos*, *Boleophthalmus boddaerti*, and *Periophthalmodon schlosseri*. *Biological Bulletin*:434-438.
Luquet C, Genovese G, Rosa G, and Pellerano G. 2002. Ultrastructural changes in the gill epithelium of the crab *Chasmagnathus granulatus* (Decapoda: Grapsidae) in diluted and concentrated seawater. *Marine Biology* 141:753-760.
Maina JN. 1990a. The morphology of the gills of the freshwater African crab *Potamon niloticus* (Crustacea: Brachyura: Potamonidae): A scanning and transmission electron microscopic study. *Journal of Zoology* 221:499-515.
Maina JN. 1990b. The morphology of the gills of the freshwater African crab *Potamon niloticus* (Crustacea: Brachyura; Potamonidae): A scanning and transmission electron microscopic study. *Journal of Zoology* 221:499-515.
Maina JN. 2000a. Comparative respiratory morphology: themes and principles in the design and construction of the gas exchangers. *Anatomical Record (New Anatomist)* 261:25-44.
Maina JN. 2000b. Is the sheet-flow design a 'frozen core'(a Bauplan) of the gas exchangers?: Comparative functional morphology of the respiratory microvascular systems: illustration of the geometry and rationalization of the fractal properties. *Comparative Biochemistry and Physiology-Part A: Molecular & Integrative Physiology* 126:491-515.
Maina JN. 2002a. Sheet flow design in the vasculature of gas exchangers. In: Maina JN, ed. *Fundamental Structural Aspects and Features in the Bioengineering of the Gas Exchangers: Comparative Perspectives*. Berlin; Heidelberg; New York; Barcelona; Hong Kong; London; Milan; Paris; Tokyo: Springer, 47-49.
Maina JN. 2002b. Structure, function and evolution of the gas exchangers: comparative perspectives. *Journal of Anatomy* 201:281-304.
Maina JN, and West JB. 2005. Thin and strong! The bioengineering dilemma in the structural and functional design of the blood-gas barrier. *Physiological Reviews* 85:811-844.
Manganaro M, Laurà R, Guerrera MC, Lanteri G, Zaccone D, and Marino F. 2012. The morphology of gills of *Haliotis tuberculata* (Linnaeus, 1758). *Acta Zoologica* 93:436-443.

McDonald DG, Cavdek V, and Ellis R. 1991. Gill design in freshwater fishes: interrelationships among gas exchange, ion regulation, and acid-base regulation. *Physiological Zoology* 64:103-123.

McNamara JC, and Faria SC. 2012. Evolution of osmoregulatory patterns and gill ion transport mechanisms in the decapod Crustacea: A review. *Journal of Comparative Physiology B* 182:997-1014.

Mohandas A, Cheng TC, and Cheng JB. 1985. Mechanism of lysosomal enzyme release from *Mercenaria mercenaria* granulocytes: A scanning electron microscope study. *Journal of Invertebrate Pathology* 46:189-197.

Mu H, Sun J, Heras H, Chu KH, and Qiu J-W. 2017. An integrated proteomic and transcriptomic analysis of perivitelline fluid proteins in a freshwater gastropod laying aerial eggs. *Journal of Proteomics* 155:22-30.

Nicaise G. 1973. The gliointerstitial system of molluscs. *International Review of Cytology*. Academic Press: Elsevier, 251-332.

Nuwayhid M, Davies PS, and Elder H. 1978. Gill structure in the common limpet *Patella vulgata*. *Journal of the Marine Biological Association of the United Kingdom* 58:817-823.

Ottaviani E. 1991. Tissue distribution and levels of natural and induced serum lysozyme immunoreactive molecules in a freshwater snail. *Tissue and Cell* 23:317-324.

Pickett JA, and Edwardson JM. 2006. Compound exocytosis: mechanisms and functional significance. *Traffic* 7:109-116.

Ponder WF, and Lindberg DR. 1997. Towards a phylogeny of gastropod molluscs: an analysis using morphological characters. *Zoological Journal of the Linnean Society* 119:83-265.

Rebelo MdF, Figueiredo EdS, Mariante RM, Nóbrega A, de Barros CM, and Allodi S. 2013. New insights from the oyster *Crassostrea rhizophorae* on bivalve circulating hemocytes. *PLoS ONE* 8:e57384.

Robson GC. 1922. Notes on the respiratory mechanism of the Ampullariidae. *Proceedings of the Zoological Society of London* pt. 1-2:341-346.

Rodriguez C, Prieto GI, Vega IA, and Castro-Vazquez A. 2018. Assessment of the kidney and lung as immune barriers and hematopoietic sites in the invasive apple snail *Pomacea canaliculata*. *PeerJ* 6:e5789. 10.7717/peerj.5789

Ruthensteiner B. 2008. Soft Part 3D visualization by serial sectioning and computer reconstruction. *Zoosymposia* 1:63-100.

Ruthensteiner B, and Hess M. 2008. Embedding 3D models of biological specimens in PDF publications. *Microsc Res Tech* 71:778-786. 10.1002/jemt.20618

Salvini-Plawen L, and Haszprunar G. 1987. The Vetigastropoda and the systematics of streptoneurous Gastropoda (Mollusca). *Journal of Zoology* 211:747-770.

Seuffert ME, and Martín PR. 2010. Dependence on aerial respiration and its influence on microdistribution in the invasive freshwater snail *Pomacea canaliculata* (Caenogastropoda, Ampullariidae). *Biological Invasions* 12:1695-1708. 10.1007/s10530-009-9582-5

Stern DL. 2013. The genetic causes of convergent evolution. *Nature Reviews Genetics* 14:751.

Taylor P, and Andrews EB. 1987. Tissue adenosine-triphosphatase activities of the gill and excretory system in mesogastropod molluscs in relation to osmoregulatory capacity. *Comparative Biochemistry and Physiology Part A: Physiology* 86:693-696.

729 Ueshima E, and Yusa Y. 2014. Antipredator behaviour in response to single or combined
730 predator cues in the apple snail *Pomacea canaliculata*. *Journal of Molluscan*
731 *Studies*:eyu057.
732 Vega IA, Damborenea M, Gamarra-Luques C, Koch E, Cueto J, and Castro-Vazquez A. 2006.
733 Facultative and obligate symbiotic associations of *Pomacea canaliculata*
734 (Caenogastropoda, Ampullariidae). *Biocell* 30:367-375.
735 Wanichanon C, Laimek P, Linthong V, Sretarugsa P, Kruatrachue M, Upatham ES, Poomtong T,
736 and Sobhon P. 2004. Histology of hypobranchial gland and gill of *Haliotis asinina*
737 Linnaeus. *Journal of Shellfish Research* 23:1107-1113.
738 Wilson JM, and Laurent P. 2002. Fish gill morphology: inside out. *Journal of Experimental*
739 *Zoology* 293:192-213.
740 Yu AS. 2017. Paracellular transport as a strategy for energy conservation by multicellular
741 organisms? *Tissue Barriers* 5:2509-2518.

Figure 1

The gill and the mantle complex.

(A) Diagram of the mantle cavity of a male animal, opened as indicated in the thumbnail sketch at the right lower corner. (B) Panoramic section of the single row of rather parallel leaflets of the monopectinate gill that hang from the gill's base, below the outer mantle; the approximate position of this section is indicated in the thumbnail sketch at the right lower corner. Haematoxylin–eosin. Scale bar represents 1 mm. Abbreviations: abv, afferent branchial vessel; anu, anus; gil, gill; dig, digestive gland; epb, efferent pulmobranchial vessel; ime, inner mantle epithelium; kid, kidney; lft, gill leaflets; lng, lung; med, mantle edge; mfo, mantle fold; mth, mouth; ome, outer mantle epithelium; osp, osphradium; pec, penile complex; pes, penile sheath; pne, pneumostome; pod, foot; rnl, right nuchal lobe; prc, pericardium; pro, prostate; sip, siphon; ten, tentacle; tes, testicle; upo, urinary pore; urt, ureter; vap, ventral afferent pulmonary vessel.

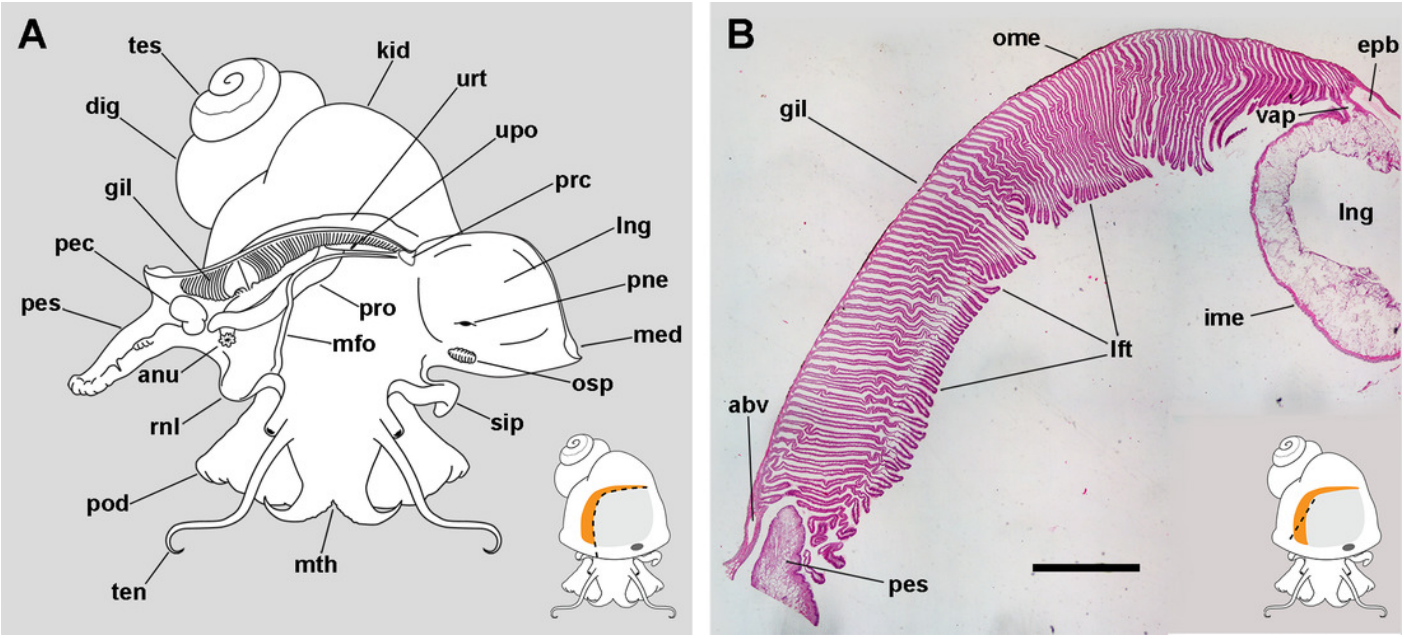

Figure 2

Computerised 3D rendering of the gill circulation.

(A) Dorsal view of the dissection piece: the gill (orange) occupies the right and posterior portion of the roof of the mantle cavity, limiting with the lung (which is collapsed, see Methods) and with the ureter. (B) Lateral view of a single gill leaflet. (C) The gill's blood supply; three gill leaflets are indicated by asterisks. (D) Blood sinuses in a single gill leaflet. (E) Diagram of the proposed blood flow to and from the gill. (F) Diagram of proposed blood flow within a gill leaflet. Scale bars represent: (A and C) 1 mm; (B and D) 500 µm. Abbreviations: abv, afferent branchial vessel; apv, afferent pulmonary vessel; aur, auricle; bls, basal leaflet sinus; gil, gill; epv, efferent pulmobranchial vessel; euv, efferent ureteral vessel; lfs, laminar leaflet sinus; lft, gill leaflet; lng, lung; med, mantle edge; mls, marginal leaflet sinus; osp, osphradium; pne, pneumostome; rct, rectum; rps, right pallial sinus; rsi, rectal sinuses; upo, urinary pore; urt, ureter; vap, ventral afferent pulmonary vessel.

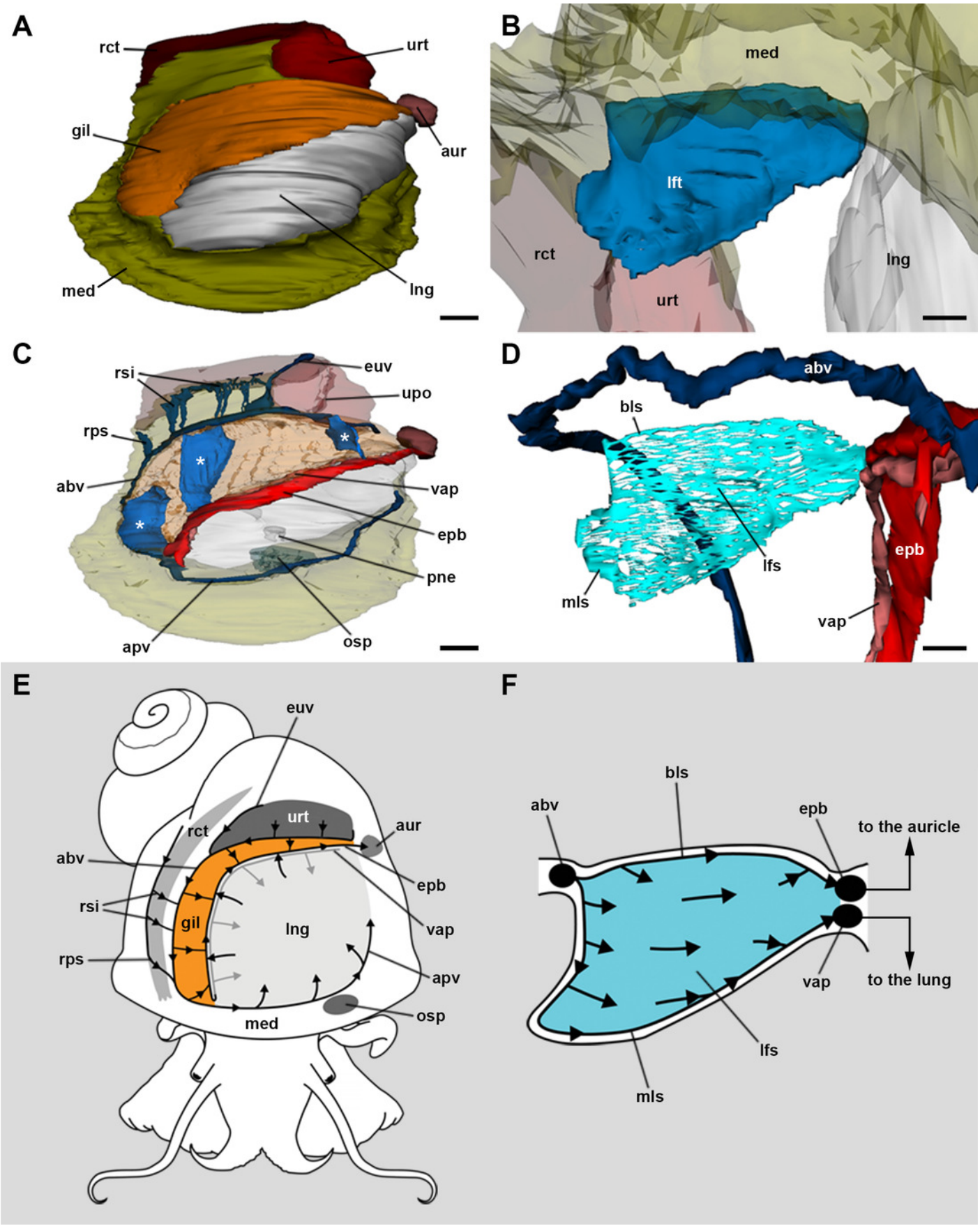
A
rct
urt
gil
aur
med
lng
B
med
lft
rct
lng
urt
C
rsi
euv
upo
rps
*
*
*
abv
vap
epb
pne
apv
osp
D
abv
bls
lfs
epb
mls
vap
E
euv
rct
urt
aur
abv
epb
rsi
gil
lng
vap
rps
apv
med
osp
F
bls
abv
epb
to the auricle
vap
to the lung
lfs
mls

Figure 3

Gill innervation.

(A) Diagram showing central ganglia (grey), and the nerves and accessory ganglia supplying branchial innervation. The gill is innervated from the supraintestinal ganglion by branches of the branchial nerve (pink). The branchial base nerve originates in the accessory supraintestinal ganglion (violet). The copulatory ganglion may also contribute to branchial innervation (green). (B) Diagram of nerves within each gill leaflet and presumptive origin of the fine innervation (dashed lines). (C) Panoramic section of the gill, showing the branchial base nerve lying alongside the afferent branchial vessel. (D) Detail of the penile complex, showing the copulatory ganglion in the proximity of the branchial base nerve. (E) Detail of the gill base showing the branchial base nerve and the afferent branchial vessel. (F) Detail showing the branchial base nerve in the proximity of the efferent ureteral vessel. Haematoxylin–eosin; panels D–F correspond to sections adjacent to that in panel C. Scale bars represent: (C) 1 cm; (D) 1 mm; (E–F) 500 µm. Abbreviations: abv, afferent branchial vessel; asg, accessory supraintestinal ganglion; bbn, branchial base nerve; brn, branchial nerve; cog, copulatory ganglion; euv, efferent ureteral vessel; lfn, leaflet nerve; lft, gill leaflet; ome, outer mantle epithelium; osg, osphradial ganglion; pec, penile complex; pes, penile sheath; rpg, right pleural ganglion; rps, right pallial sinus; sig, supraintestinal ganglion; urt, ureter; vig, visceral ganglion; vsc, viscero–supraintestinal connective.

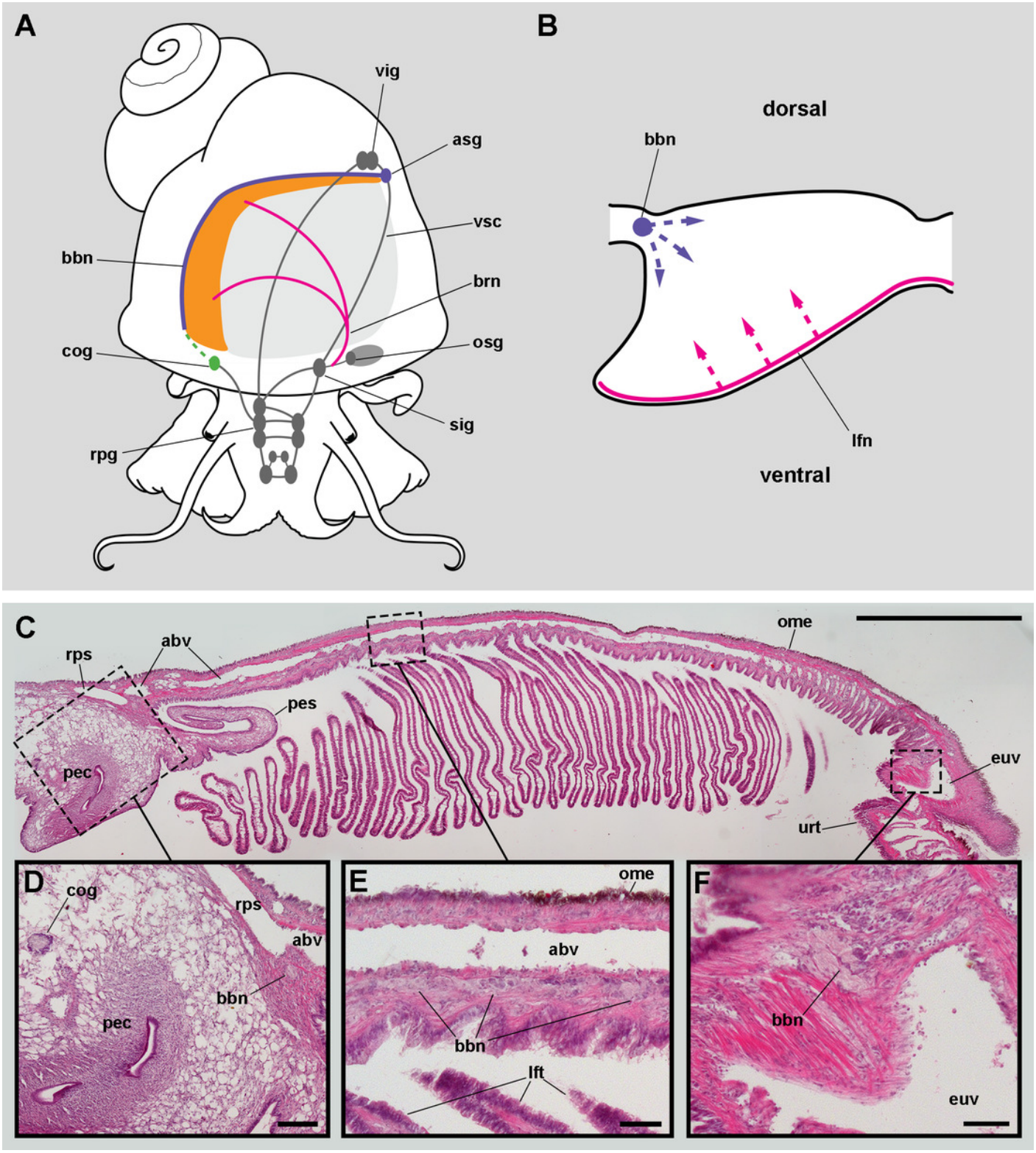
A
vig
asg
vsc
bbn
brn
cog
osg
sig
rpg
B
dorsal
bbn
lfn
ventral
C
rps
abv
ome
pes
pec
euv
urt
D
cog
rps
abv
bbn
pec
E
ome
abv
bbn
lft
F
bbn
euv

Figure 4

The gill leaflet and its regions (light microscopy).

(A) Diagram of the four regions of a gill leaflet, which differ in the cell types of its covering epithelium and underlying structures. (B–C) Region I occupies the largest part of the leaflet, while regions II–IV. (D–E) constitute its thickened margin. Scale bars represent 20 µm. Haematoxylin-eosin or toluidine blue. Abbreviations: bls, basal leaflet sinus; cil, cilia; fml, fibromuscular layer; gra, granulocytes; ics, intercellular spaces; lfn, leaflet nerve; lfs, laminar leaflet sinus; mls, marginal leaflet sinus; nuc, epithelial cell nuclei; ome, outer mantle epithelium; rod, skeletal rod; sec, secretory cells; tra, trabeculae.

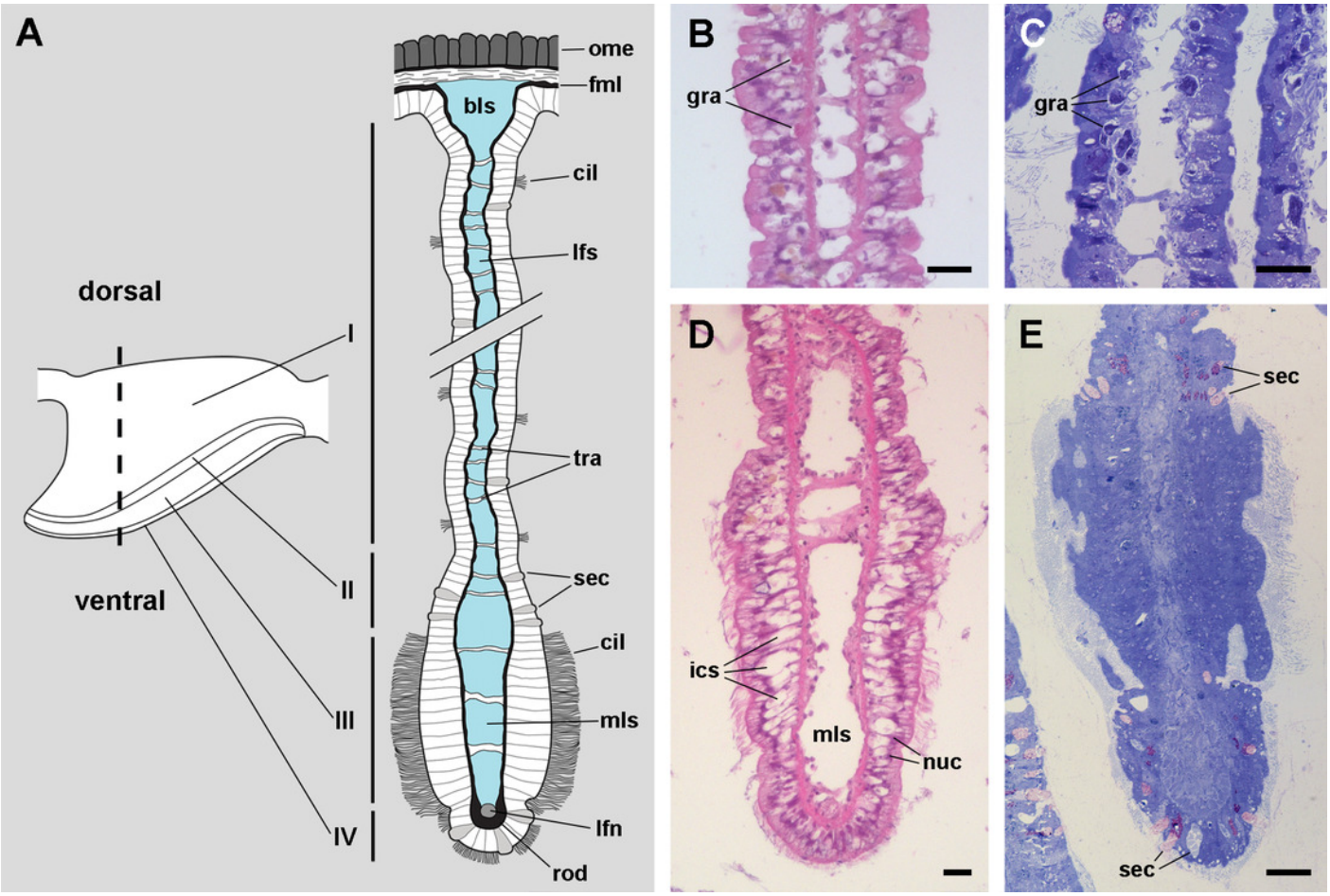

Figure 5

Apical specialisations on the gill surface (scanning electron microscopy).

(A) Piece of dissection of three adjacent gill leaflets, two of them sectioned to show the laminar leaflet sinus. Regions described in Fig. 4A are indicated in the thumbnail sketch. (B) Region I exhibiting the cilia of α-cells and the ramified microvilli of β-cells. (C) Region III exhibiting the long cilia of C2 cells with the characteristic membrane blebs. (D) Region IV exhibiting bundles of the short cilia of C1 cells, and interspersed spaces showing the microvilli of α-cells. (E) A cut through region I of a gill leaflet, showing the laminar leaflet sinus, the trabeculae traversing it, and the covering leaflet epithelia showing α-cells, β-cells and C1 cells. Scale bars represent: (A) 200 µm; (B) 10 µm; (C–E) 2 µm. Abbreviations: α, α-cells; β, β-cells; C1, short cilia cells; lfs, laminar leaflet sinus; mbl, membrane blebs on the long cilia; tra, trabeculae.

**Note: Auto Gamma Correction was used for the image. This only affects the reviewing manuscript. See original source image if needed for review.*

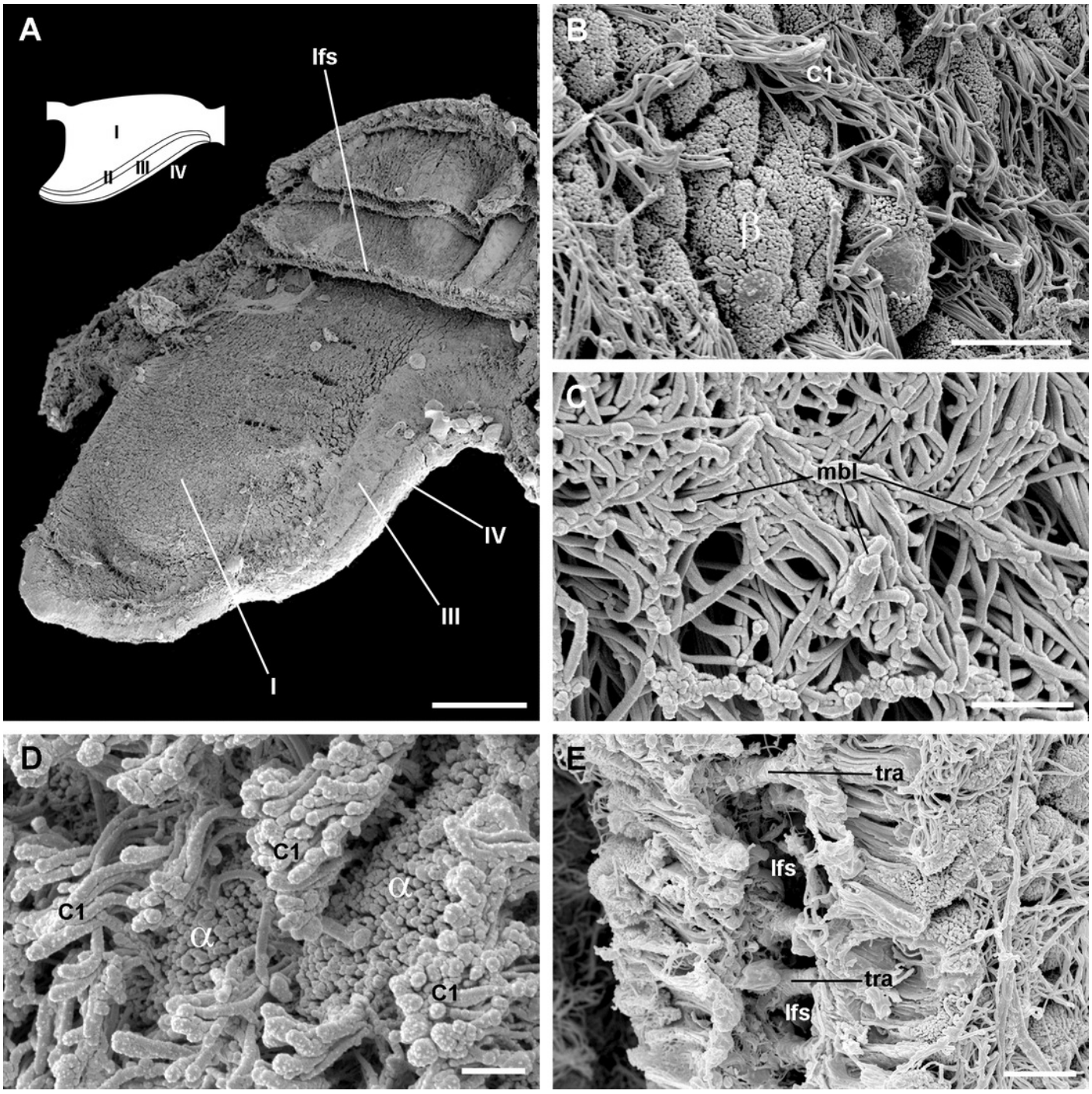
A
lfs
I
II
III
IV
IV
III
I
B
C1
β
C
mbl
D
C1
C1
α
α
C1
E
tra
lfs
tra
lfs

Figure 6

Mitochondria-rich cells in region I of a gill leaflet (diagram).

The two main cell types found in region I are α- and β-cells. In addition, granulocytes occur within epithelial intercellular spaces. Abbreviations: adh, adherent junction; α-c, alpha-cell; β-c, beta-cell; bla, basal lamina; dtu, bundles of electron-dense tubules; gra, granulocyte; grn, R granules; fgr, fibrogranular figure; gly, glycogen deposit; icc, intercellular canaliculi; mlb, multilamellar bodies; mvb, multivesicular bodies; mvi, microvilli; mye, myeloid figure; neu, neurite bundle; sep, septate junction; tep, thin epithelial projections; tub, tubular system.

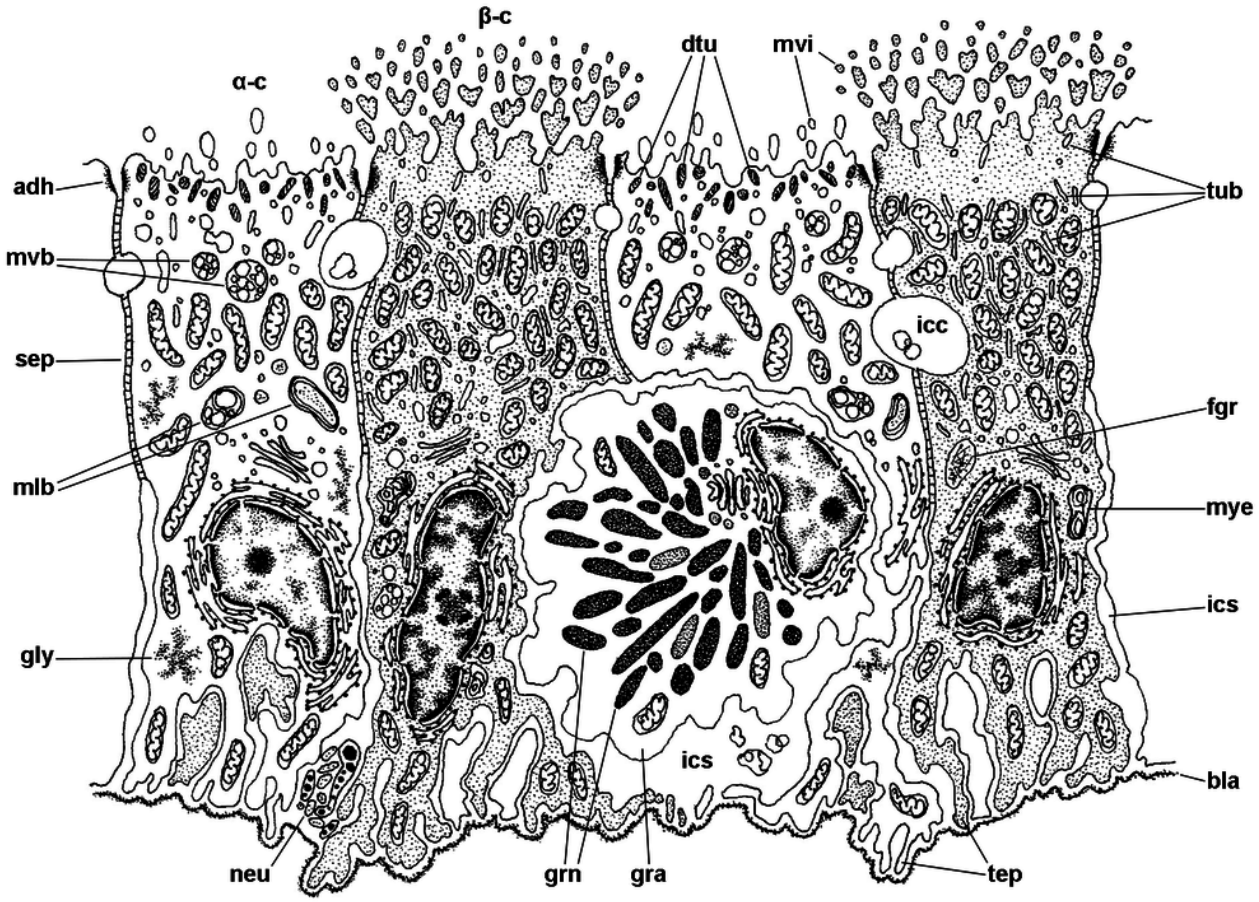

Figure 7

Mitochondria-rich cells in region I of a gill leaflet (transmission electron microscopy).

(A) Alpha-cells exhibit few and short microvilli, numerous and long mitochondria with well-defined cristae, and glycogen deposits. Their nuclei are euchromatic with conspicuous nucleoli. (B) Apically, α-cells show numerous membrane-bound bundles of electron-dense tubules/filaments, and a well-developed vesicular system, including multivesicular bodies. (C) Multilamellar bodies and Golgi bodies are found close to the nucleus. (D) Contrasting with α-cells, β-cells have numerous and ramified microvilli. These cells also have numerous tightly-packed mitochondria that fill almost all the cytoplasm. The nuclei are heterochromatic. (E) Beta-cells show an extensive tubular system between the mitochondria. (F) A β-cell showing multivesicular bodies and presumptively degenerative bodies, such as myeloid and fibrogranular figures. Scale bars represent: (A) 1 µm; (B) 200 nm; (C) 250 nm; (D) 1 µm; (E) 500 nm; (F) 250 nm. Abbreviations: α-c, alpha-cell; β-c, beta-cell; dtu, bundles of electron-dense tubules; fgr, fibrogranular figure; gly, glycogen deposit; gol, Golgi body; gra, granulocyte; icc, intercellular canaliculi; mit, mitochondria; mlb, multilamellar body; mvb, multivesicular body; mvi, microvilli; mye, myeloid figure; nuc, cell nucleus; rer, rough endoplasmic reticulum; tep, thin epithelial projections; tub, tubular-vesicular system.

**Note: Auto Gamma Correction was used for the image. This only affects the reviewing manuscript. See original source image if needed for review.*

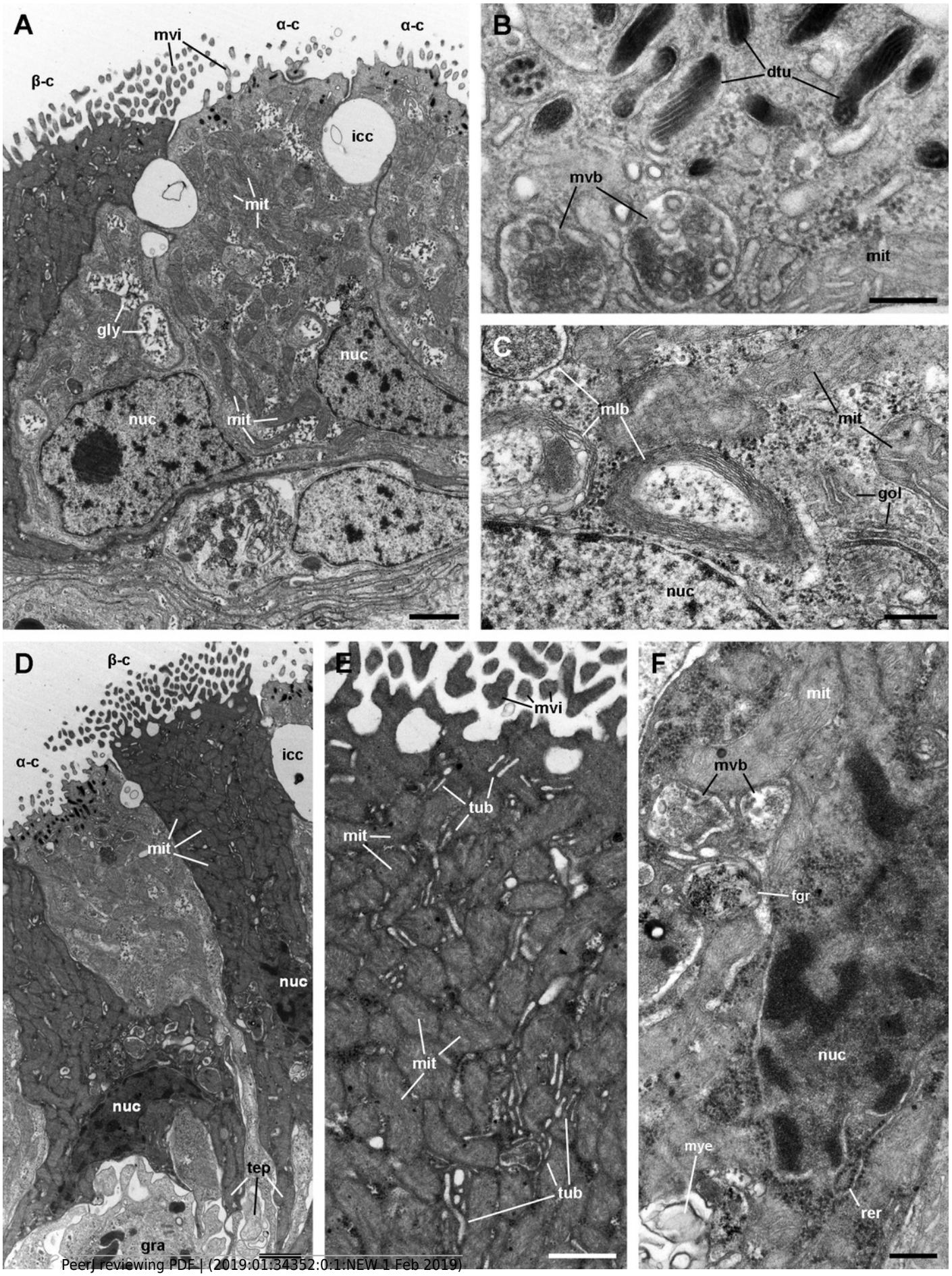
A
mvi
α-c
α-c
β-c
icc
mit
gly
nuc
nuc
mit
B
dtu
mvb
mit
C
mlb
mit
gol
nuc
D
β-c
α-c
icc
mit
nuc
nuc
tep
gra
E
mvi
tub
mit
mit
tub
F
mit
mvb
fgr
nuc
mye
rer

Figure 8

Structures associated with granulocytes in the basolateral domain of the gill epithelium (transmission electron microscopy).

(A) Labyrinth of thin cellular extensions projecting towards the collagen matrix of the underlying connective tissue, where sparse muscle fibres occur. Subepithelial and intraepithelial (arrows) neurite bundles with accompanying glial cells also occur. (B) A granulocyte in close proximity to the basal lamina occupies an enlarged intercellular space. Small intercellular spaces or canaliculi are also seen. (C) Discontinuities in the basal mesh of epithelial projections communicate the intercellular spaces directly with the basal lamina, which shows interspersed electron dense thickenings (arrowheads). (D) Basolateral infoldings of an α-cell, adjacent to a β-cell. Scale bars represent: (A–B) 2 µm; (C) 1 µm; (D) 500 nm. Abbreviations: bla, basal lamina; bsi, blood sinus; col, collagen matrix; gra, granulocyte; grn, R granule; icc, intercellular canaliculi; ics, intercellular space; msc, muscle cell; neu, neurite bundle; tep, thin epithelial projections.

**Note: Auto Gamma Correction was used for the image. This only affects the reviewing manuscript. See original source image if needed for review.*

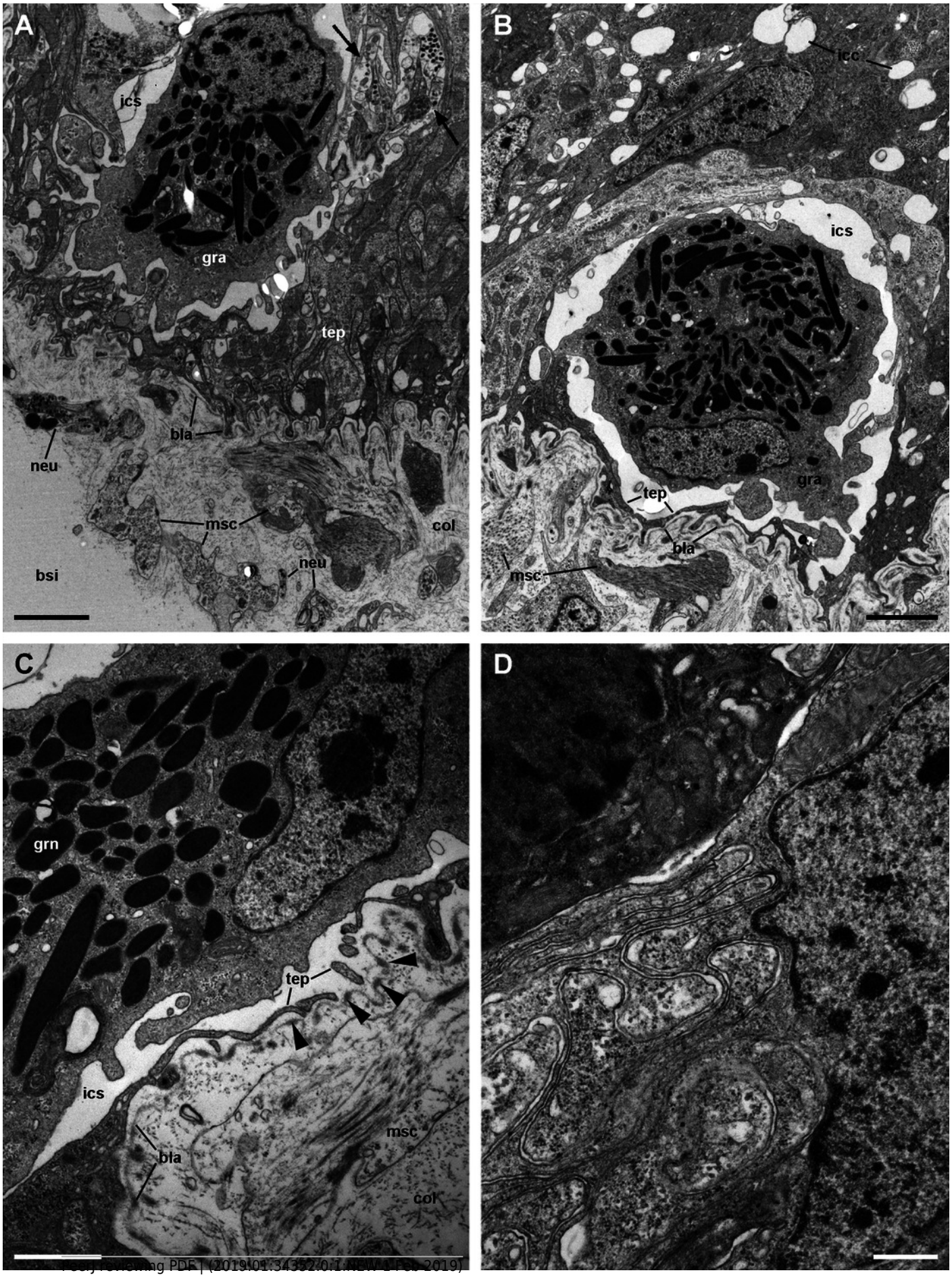
A
ics
gra
tep
bla
neu
msc
col
neu
bsi
B
icc
ics
gra
tep
bla
msc
C
grn
tep
ics
msc
bla
col
D

Figure 9

Long cilia cells (C2) in region III of a gill leaflet (transmission electron microscopy).

A) Diagram. (B) C2 cells exhibit an electron dense cytoplasm with abundant rough endoplasmic reticulum and glycogen deposits. These cells rest on a thick and electron dense basal lamina (arrowheads). There are extensive intercellular spaces and smaller canaliculi, also seen under light microscopy (Figure 4D). (C) Transverse section of a cilium shows the typical 9+2 microtubule arrangement and membrane blebs (arrows). (D) Membrane-bound bundles of electron-dense tubules/filaments in the apical domain of a C2 cell. Scale bars represent: (B) 1 µm; (C) 50 nm; (D) 250 nm. Abbreviations: adh, adherent junction; bla, basal lamina; cil, cilia; dtu, bundles of electron-dense tubules; gly, glycogen deposit; icc, intercellular canaliculi; ics, intercellular space; msc, muscle cell; mtb, microtubules; mvi, microvilli; neu, neurite bundle; rer, rough endoplasmic reticulum; sep, septate junction; tep, thin epithelial projections.

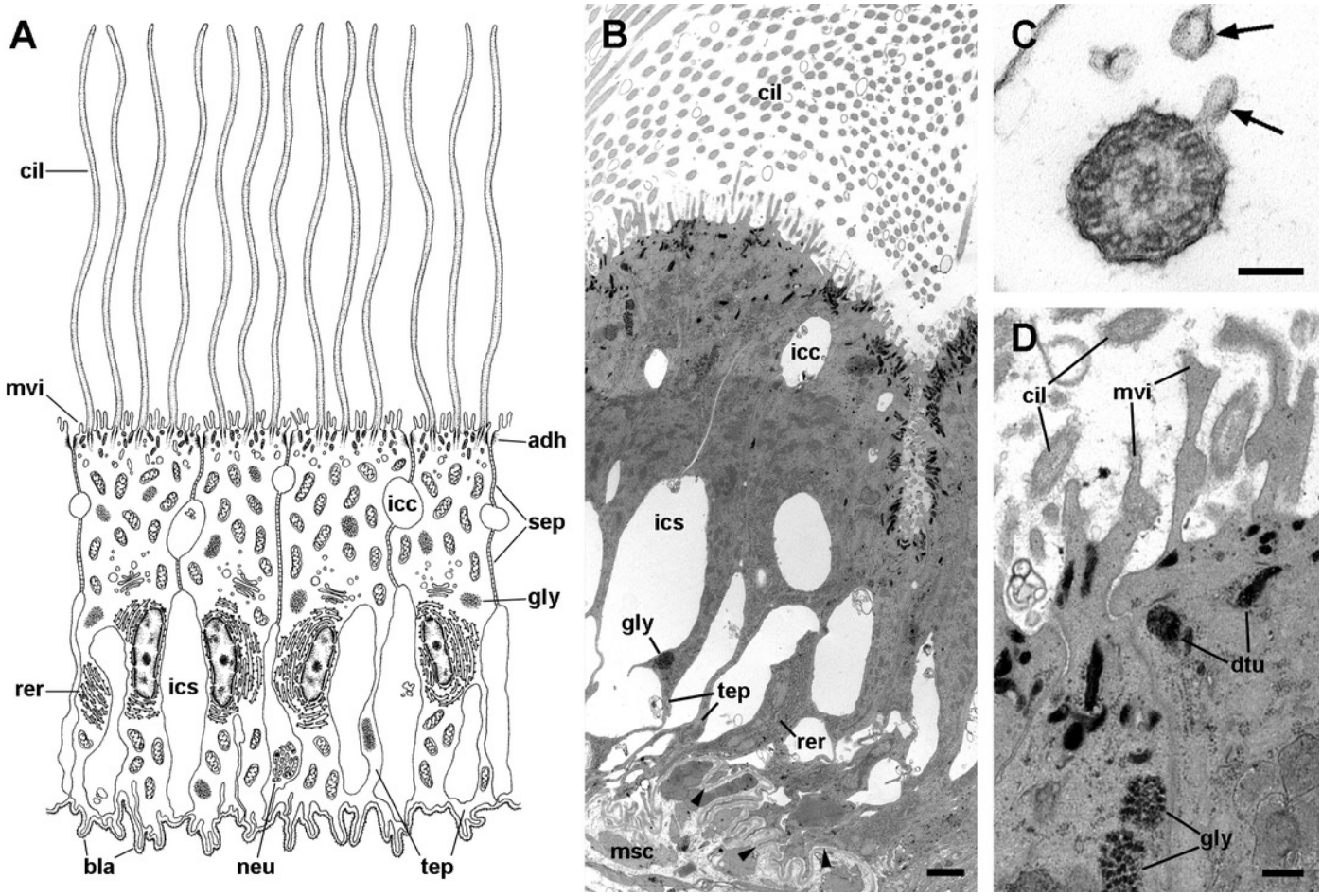
A
cil
mvi
adh
icc
sep
gly
rer
ics
bla
neu
tep
B
cil
icc
ics
gly
tep
rer
msc
C
D
cil
mvi
dtu
gly

Figure 10

Ciliary (C1) and secretory (S1 and S2) cells in region IV of a gill leaflet (transmission electron microscopy).

(A) Diagram. (B) C1 cells exhibit a moderately electron-dense cytoplasm containing large dense-cored granules and a heterochromatic nucleus. Apically, there are finger-like microvilli and short cilia with membrane blebs. Glycogen deposits are also found. (C) An S1 cell showing granules above the nucleus, which contain an inner electron-dense mesh. (D) An S1 cell showing a large accumulation of granules with a looser electron-dense mesh, in the apex. (E) An S2 cell with the cytoplasm almost filled with vacuoles containing a microgranular substance of moderate electron density. Scale bars represent: (B) 1 µm; (C) 500 nm; (D–E) 1 µm. Abbreviations: adh, adherent junction; bla, basal lamina; cil, cilia; dcg, dense-core granules; dtu, bundles of electron-dense tubules; gly, glycogen deposit; icc, intercellular canaliculi; ics, intercellular space; mug, mucinogen granules; mvb, multivesicular body; mvi, microvilli; neu, neurite bundle; nuc, cell nucleus; sep, septate junction; tep, thin epithelial projections; vac, vacuolae.

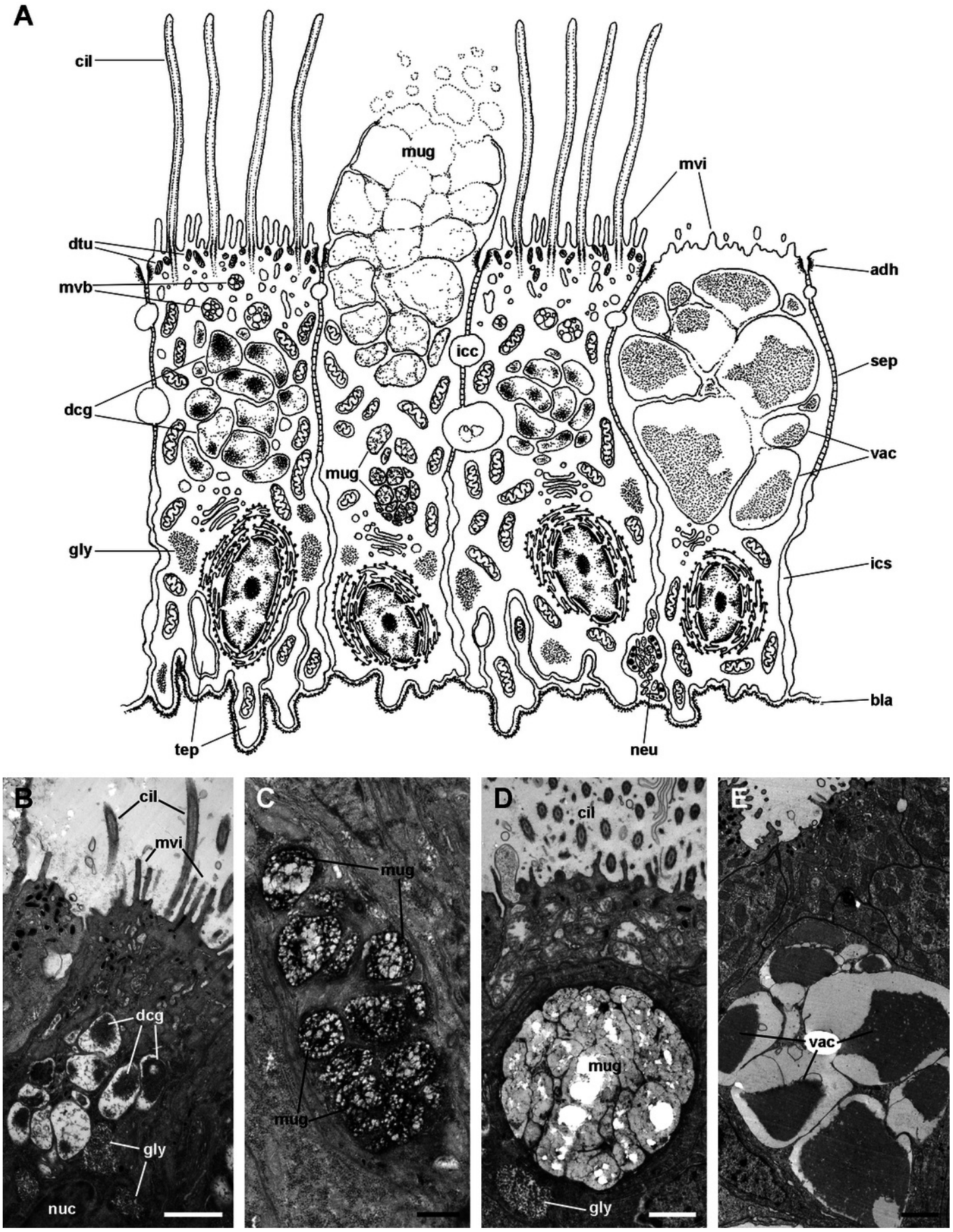
A
cil
mug
mvi
dtu
mvb
adh
icc
sep
dcg
vac
mug
gly
ics
bla
tep
neu
B
cil
mvi
dcg
gly
nuc
C
mug
mug
D
cil
mug
gly
E
vac

Figure 11

Cell junctions (transmission electron microscopy).

(A) Apical adherent junction followed by a short septate junction and an intercellular canaliculum with some content. (B) A septate junction. (C) Widening of an intercellular space below the septate junction. Scale bars represent 200 nm. Abbreviations: adh, adherent junction; dtu, bundles of electron-dense tubule; icc, intercellular canaliculi; ics, intercellular space; mit, mitochondrion; sep, septate junction; tub, tubular system.

**Note: Auto Gamma Correction was used for the image. This only affects the reviewing manuscript. See original source image if needed for review.*

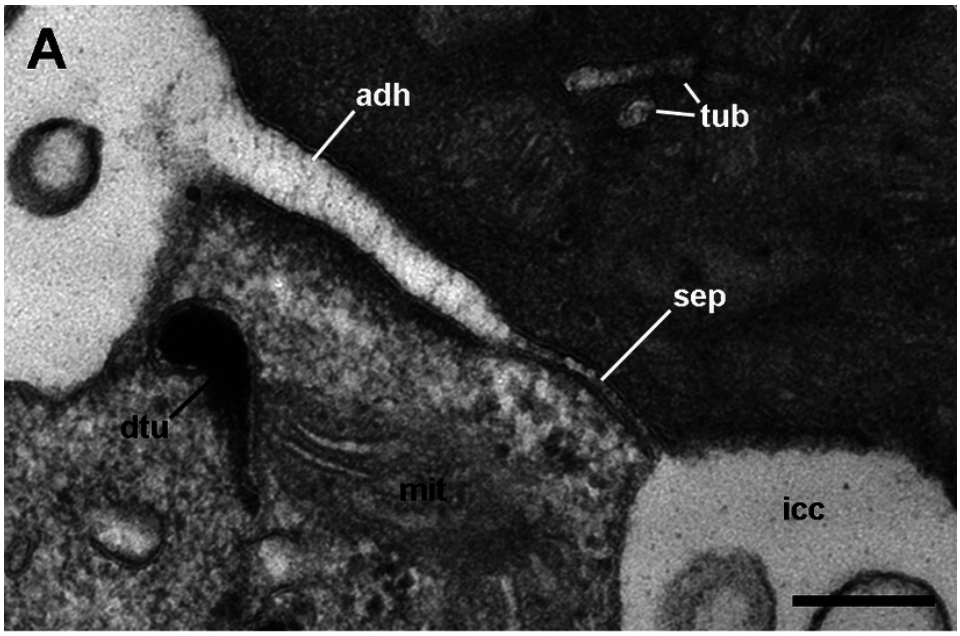
A
adh
tub
sep
dtu
mit
icc

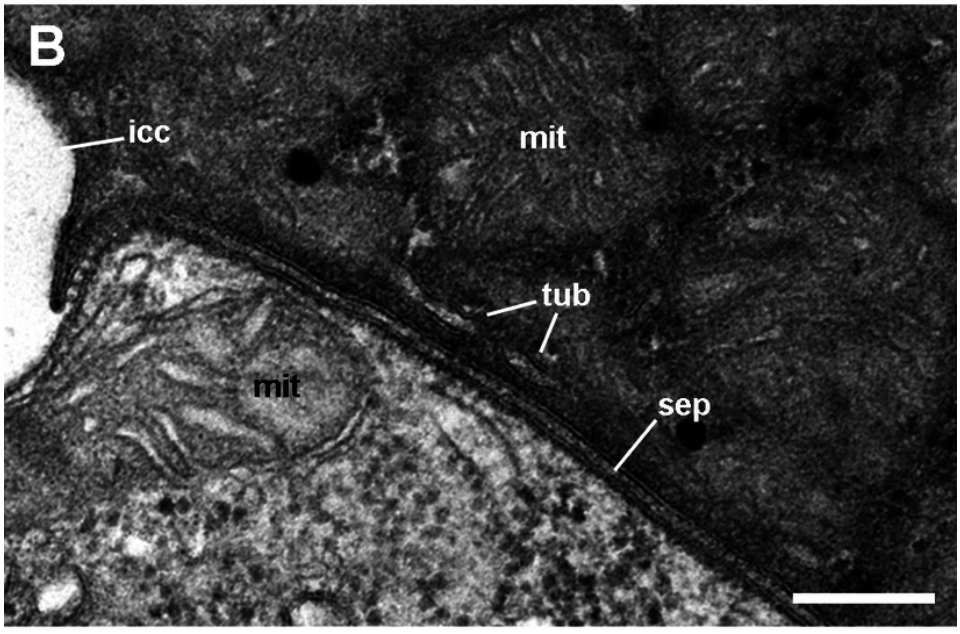
B
icc
mit
tub
mit
sep

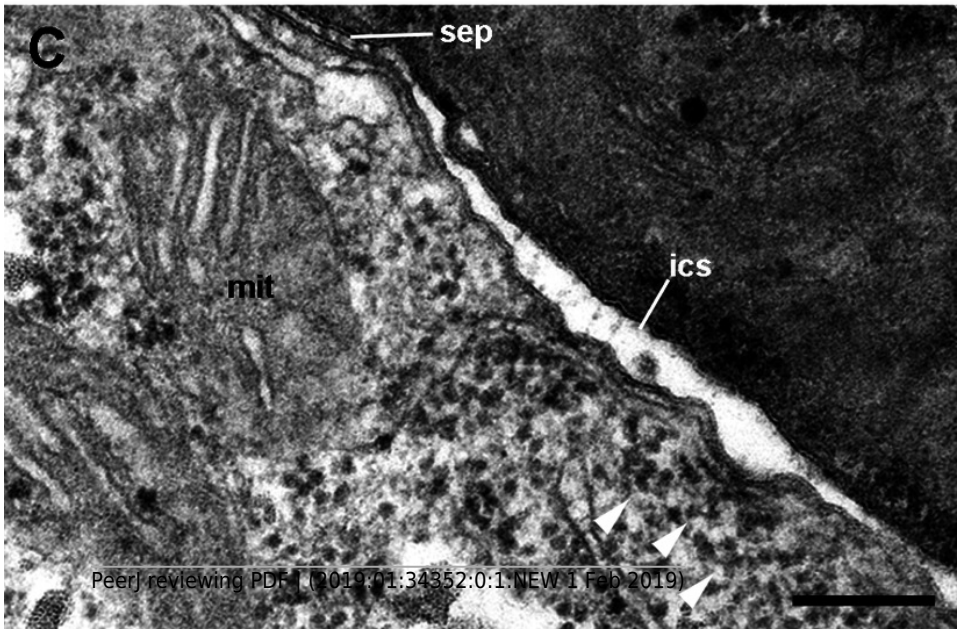
C
sep
ics
mit

Figure 12

Fibromuscular tissue and fine innervation of the gill leaflets (transmission electron microscopy).

(A) Overview of the basal domain of epithelial cells, together with a granulocyte in contact with the basal lamina (arrowheads). The underlying tissue exhibits a neurite/glial bundle and trabecular fibromuscular cells with inner myofibrils and electron-dense anchoring junctions with the collagen matrix and the basal lamina. Also notice some intraepithelial neurites (white arrows). (B) Detail of anchoring junctions showing the external brush-like plaque and the internal amorphous electron-dense layer. (C) Detail of a neurite bundle showing neurites associated with glial cells' processes containing granules of different sizes and electron density. Glial cells, or rarely uncovered neurite bundles, are in contact with muscle fibres or trabeculae. Scale bars represent: (A) 1 µm; (B) 500 nm; (C) 500 nm. Abbreviations: anc; anchoring junction; cav, caveolae; col, collagen matrix; gcp, glial cell process; gra, granulocyte; ics, intercellular space; mit, mitochondria; msc, muscle cells; myo, myofibrils; nee, presumptive nerve endings; neu, neurite bundles; tep, thin epithelial projection.


A
ics
gra
tep
tep
msc
col
neu
mit

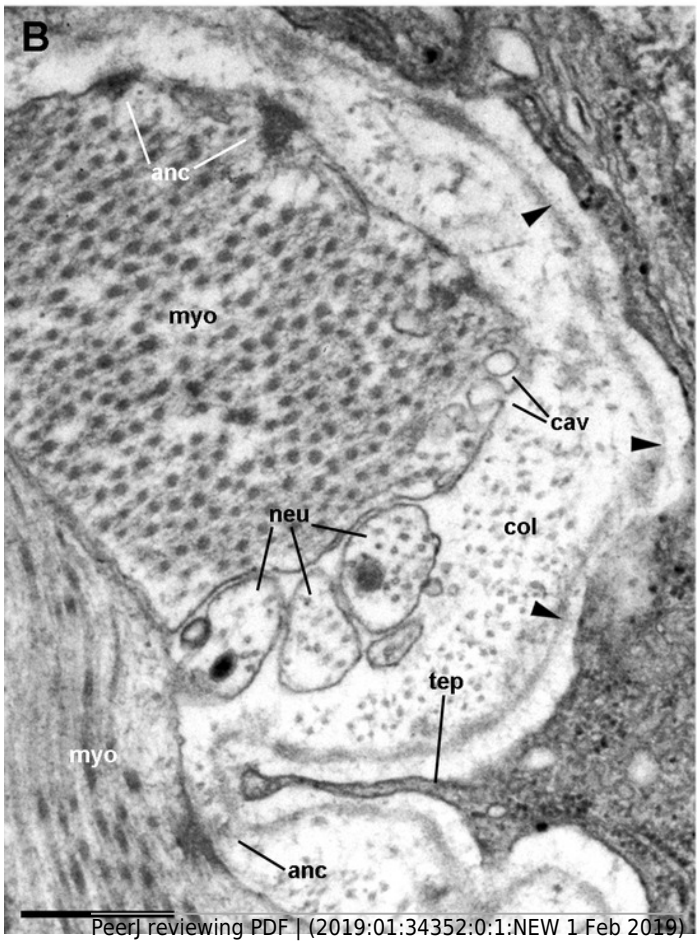
B
anc
myo
cav
neu
col
tep
myo
anc

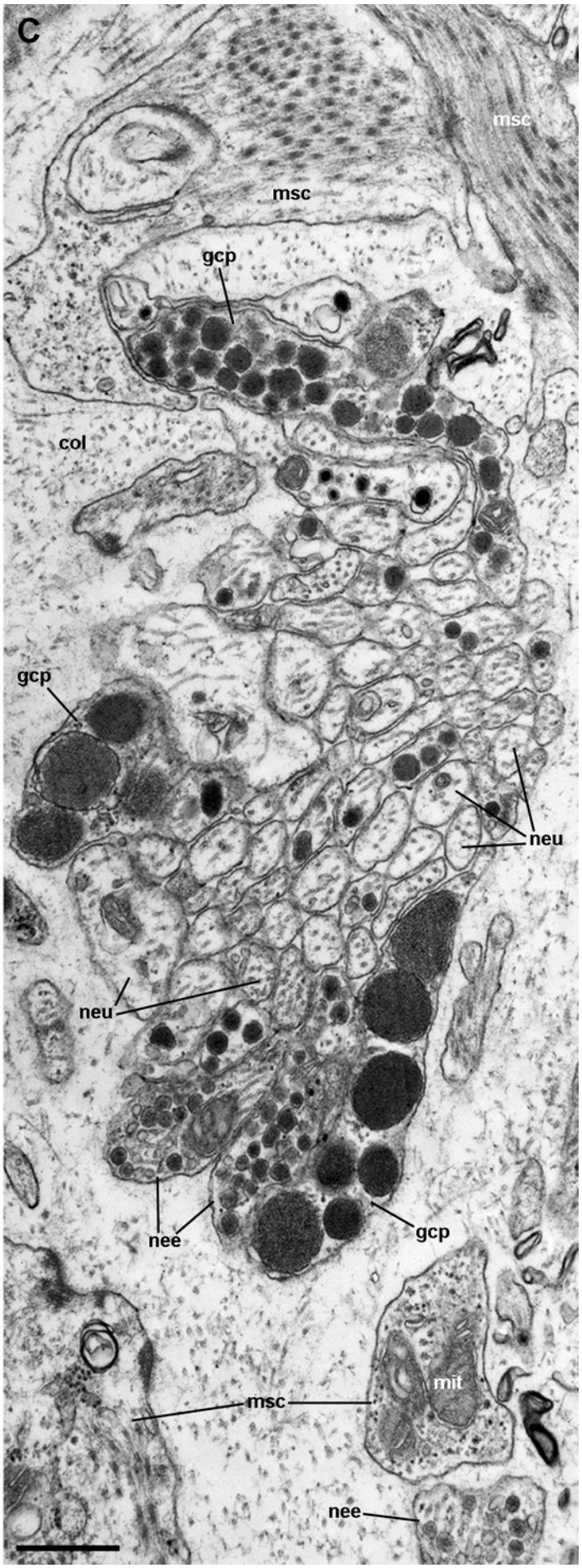
C
msc
msc
gcp
col
gcp
neu
neu
nee
gcp
mit
msc
nee

Figure 13

The skeletal rod and the leaflet nerve (light and electron microscopy).

(A) Margin of a gill leaflet showing the covering epithelium, the skeletal rod and the leaflet nerve. Toluidine blue. (B) Razor blade cuts of three gill leaflets showing the skeletal rods as well-defined units beneath the covering epithelium. Scanning electron microscopy. (C) Tangential section of the leaflet border showing two muscular cells pertaining to the skeletal rod and a fairly longitudinal section of the leaflet nerve. Transmission electron microscopy. (D) A high magnification of the leaflet nerve showing tightly packed neurites containing neurotubules, clear vesicles or electron-dense granules of different sizes. (E) A section through the skeletal rod showing large muscle fibres containing myofibrils, and that are embedded in a collagen matrix where glial processes are found. Arrowheads indicate the basal lamina of the covering epithelium. Scale bars represent: (A) 10 µm; (B) 25 µm; (C–D) 1 µm; (E) 250 nm. Abbreviations: C1, short cilia cells; col, collagen matrix; gcp, glial cell process; gra, granulocyte; msc, muscle cell; mye, myeloid figure; lfn, leaflet nerve; rod, skeletal rod; S1, metachromatic secretory cells; S2, orthochromatic secretory cells.

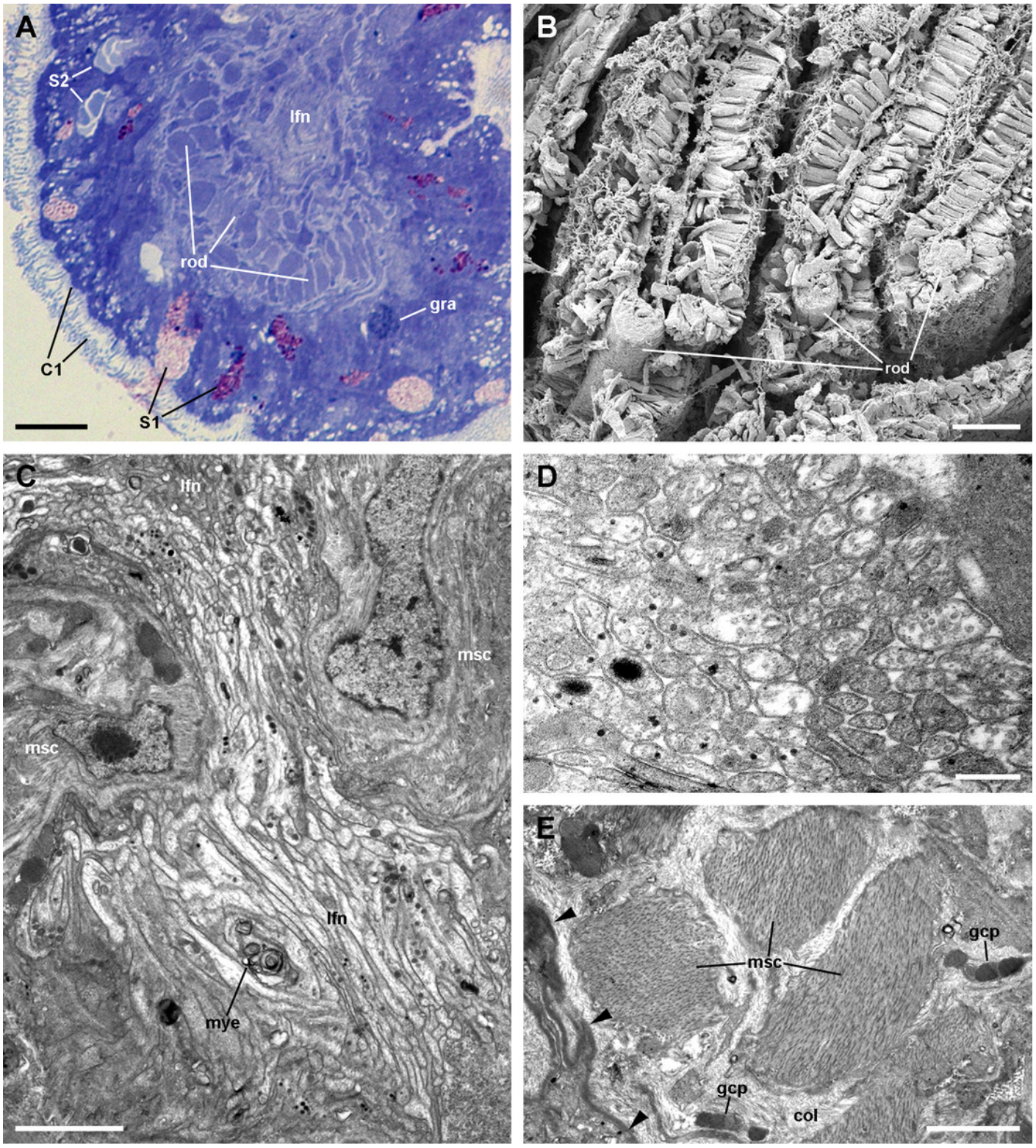
A
S2
lfn
rod
gra
C1
S1
B
rod
C
lfn
msc
msc
lfn
mye
D
E
gcp
msc
gcp
col

Table 1(on next page)

Cell types and other features of gill's leaflet regions in *P. canaliculata*.

1

Region	Epithelial cell types			Epithelial intercellular spaces	Underlying tissues
	Microvillar cells	Ciliary cells	Secretory cells		
I	α and β	C1	S1 and S2 (scarce)	Extensive spaces, with numerous granulocytes	Thin basal lamina Loose fibromuscular tissue Thin trabeculae cross the laminar leaflet sinus
II	α	None	S1 and S2 (abundant)	Narrow spaces, scarce granulocytes	Thick basal lamina Dense fibromuscular tissue Thin trabeculae cross the marginal leaflet sinus
III	None	C2	None	Extensive spaces, scarce granulocytes	Thick basal lamina Dense fibromuscular tissue Thick trabeculae cross the marginal leaflet sinus
IV	α	C1	Abundant S1 and S2	Narrow spaces, scarce granulocytes	Thick basal lamina Skeletal rod Leaflet nerve

2 Abbreviations: α, α-cells; β, β-cells; C1, short cilia cells; C2, long cilia cells; S1, metachromatic secretory
3 cells; S2, orthochromatic secretory cells.

Table 2(on next page)

Features of the cell types in the gill epithelium of *P. canaliculata*.

Cell type	Apical specialisations	Nucleus and cytoplasm	Endomembrane system	Other membrane-bound bodies
α	Few and short, finger-like microvilli	Euchromatic nucleus Abundant, long mitochondria	Abundant RER Golgi bodies Vesicular system Multivesicular bodies Multilamellar bodies	Bundles of electron-dense tubules/filaments Dense-cored granules (in region IV only)
β	Numerous and long, ramified microvilli	Heterochromatic nucleus Tightly-packed, short mitochondria	Tubular system Multivesicular bodies Myeloid and fibrogranular bodies	Few and small bundles of electron-dense tubules/filaments
C1	Short cilia with membrane blebs Short, finger-like microvilli	Heterochromatic nucleus Rather dark cytoplasm	Vesicular system Multivesicular bodies	Abundant and large dense-cored granules Bundles of electron-dense tubules/filaments
C2	Very long cilia with membrane blebs Short, finger-like microvilli	Euchromatic nucleus Rather dark cytoplasm	Abundant RER	Bundles of electron-dense tubules/filaments
S1	None	Heterochromatic nucleus Rather dark cytoplasm	Abundant RER Golgi bodies	Mucinogen granules (basally, with an electron-dense mesh; apically, with a looser electron-dense mesh)
S2	None	Euchromatic nucleus Clear cytoplasm	Abundant RER Golgi bodies	Granules with moderately electron-dense cores
G	–	Euchromatic nucleus Clear cytoplasm	Golgi bodies	R granules

Abbreviations: α, α-cells; β, β-cells; C1, short cilia cells; C2, long cilia cells; S1, metachromatic secretory cells; S2, orthochromatic secretory cells; G, granulocytes; RER, rough endoplasmic reticulum.